Paus, A., Haflidason, H., Routh, J., Naafs, B. D. A., & Thoen, M. W. (2019). Environmental responses to the 9.7 and 8.2 cold events at two ecotonal sites in the Dovre mountains, mid-Norway. *Quaternary Science Reviews*, *205*, 45-61. https://doi.org/10.1016/j.quascirev.2018.12.009

Environmental responses to the 9.7 and 8.2 cold events at two ecotonal sites in the Dovre Mountains, Mid-Norway

Aage Paus[1], Haflidi Haflidason[2], Joyanto Routh[3], B. David A. Naafs[4], and Mari W. Thoen[1]

[1]Department of Biological Science, University of Bergen, Post Box 7803, N-5020 Bergen, Norway

[2]Department of Earth Science, University of Bergen, Norway, and Bjerknes Centre for Climate Research, Norway

[3]Department of Thematic Studies – Environmental Change, Linköping University, Linköping 58183, Sweden

[4]Organic Geochemistry Unit, School of Chemistry and Cabot Institute, University of Bristol, Bristol, UK

Corresponding author:

Aage Paus,
Telephone: + 47 55 58 33 44
Fax: + 47 55 58 96 67
E-mail: aage.paus@uib.no

Key words

Early Holocene; Paleoclimatology; 9.7 and 8.2 cold events; Scandinavia; Lake sedimentology; Varves; Biomarkers; Vegetation dynamics; Ecotones

Abstract

We found strong signals of two cooling events around 9700 and 8200 cal yrs. BP in lakes Store Finnsjøen and Flåfattjønna at Dovre, mid-Norway. Analyses included pollen in both

lakes, and C/N-ratio, biomarkers (e.g. alkanes and br-GDGTs), and XRF scanning in Finnsjøen. The positions of these lakes close to ecotones (upper forest-lines of birch and pine, respectively) reduced their resilience to cold events causing vegetation regression at both sites. The global 8.2 event reflects the collapse of the Laurentide Ice Sheet. The 9.7 event with impact restricted to Scandinavia and traced by pollen at Dovre only, reflects the drainage of the Baltic Ancylus Lake. More detailed analysis in Finnsjøen shows that the events also caused increased allochtonous input (K, Ca), increased sedimentation rate, and decreased sediment density and aquatic production. br-GDGT-based temperatures indicate gradual cooling through the early Holocene. In Finnsjøen, ca. 3100 maxima-minima couplets in sediment density along the analyzed sequence of ca. 3100 calibrated years show the presence of varves for the first time in Norway. Impact of the 9.7 and 8.2 events lasted ca. 60 and 370 years, respectively. Pine pollen percentages were halved and re-established in less than 60 years, indicating the reduction of pine pollen production and not vegetative growth during the 9.7 event. The local impact of the 8.2 event *sensu lato* (ca 8420 – 8050 cal yrs. BP) divides the event into a precursor, an erosional phase, and a recovery phase. At the onset of the erosional phase, summer temperatures increased.

Introduction

The early Holocene is characterized by a series of well-documented climate instabilities, i.e. cooling episodes, that are likely driven by a slow reorganization of the North Atlantic thermohaline circulation (e.g. Andersson et al., 2004; Berner et al., 2010; Wanner et al., 2011) in combination with a decrease in summer solar insolation (Renssen et al., 2007) and probably also periodic presence of perennial Arctic sea ice cover (Stranne et al., 2014). The most prominent early Holocene cooling episodes ca. 11.300 cal yrs. BP (PreBoreal Oscillation: PBO), 9700-9300 cal yrs. BP (Erdalen 2 event *s.l.*), and 8200 cal yrs. BP (Finse event) are

included in the quasi-periodic Holocene "Bond-cycles" (Bond et al., 1997). These climatic cycles are thought to be related to perturbations in solar radiation and/or continental ice sheet dynamics (Bond et al., 2001; Obrochta et al., 2016). The three cold periods are clearly recorded in the marine stratigraphy of the North Atlantic and Nordic Seas (e.g. Koç and Jansen, 1992; Haflidason *et al.*, 1995; Björck et al., 1997; Andersen et al., 2004; Berner et al., 2008, 2010), and by glacial deposits showing glacial readvances in Scandinavia and the Alps (e.g. Nesje and Dahl., 2001; Dahl et al. 2002; Bakke et al., 2005; Nicolussi and Schlüchter, 2012; Gjerde et al., 2016; Moran et al., 2016).

The impact of these climatic events in Europe, and in particular, the impact on vegetation is less clear. Obviously, due to the remains of the decaying Weichselian Ice Sheet lingering, the records of the earliest climate oscillation are sparse in Scandinavia (Björck et al., 1997; Paus et al., 2015) compared to further south (Bos et al., 2007; Dormoy et al., 2009). In contrast, the influence on vegetation from the 8.2 event is more frequently recorded in mid- and northern Europe than southern parts of the continent (Ghilardi and O'Connell, 2013; Fiłoc et al., 2017). Nonetheless, well-established cases of this event have been identified in Spain (Davis and Stevenson, 2007), SE Europe (Budja, 2007), and as far east as Syria (van der Horn et al., 2015). Few studies document the 9.7-9.3 event, and those that do only show minor changes in vegetation (Wohlfarth et al., 2004; Whittington et al., 2015; Burjachs et al., 2016). In context of the distinct 9.7-9.3 signals recorded in marine sequences and glacial deposits, the lack of vegetation responses of similar strength and frequency in continental Europe is surprising as the underlying mechanism is thought to be the same for all events. A possible cause for the fragmented records could be low sample resolution at some sites (Whittington et al., 2015), but most probably, the lack of studies at ecotonal sites could explain the limited vegetation signal for this event. It is at the vegetation boundaries, the ecotones, that vegetation is less resilient to climate change (Smith, 1965; Fægri and Iversen, 1989), and here the strongest effects of cold events are signaled. Today, numerical treatments of large pollen-data sets find

regional patterns of vegetation and climate change (e.g. Seppä et al., 2007; Seddon et al., 2015; Hjelle et al., 2018). However, the number of sites may not be crucial for elaborating detailed geographical patterns of these events. More important is the quality of sites studied including their ecotonal positions.

This study compares multi-proxy records from two sites at Dovre (Norway): Flåfattjønna (Paus, 2010) and Finnsjøen, where the pollen data are reported by Thoen (2016). The aim is to shed new light on the question whether the early Holocene "Bond"-events impacted climate and vegetation in northern Europe. The lakes were close to ecotones (Flåfattjønna: upper pine-forest line, Finnsjøen: upper birch-forest line) during the Early Holocene, and show two short-lasting vegetation fluctuations during this period. To investigate the causes of these climatic oscillations, we use AMS-dates of terrestrial macrofossils and principle component analysis (PCA) of the Finnsjøen and Flåfattjønna pollen data, combined with XRF-scanning, elemental (C/N) ratio, and biomarker (glycerol diakyl glycerol tetraethers (GDGT) and *n*-alkane) analyses.

2. Regional setting

The Dovre mountain ridge with Lake Store Finnsjøen is situated between the valleys Drivdalen and Vinstradalen in Oppdal, Trøndelag County (Norway) (Fig. 1). Lake Flåfattjønna lies 30 km to the east of the ridge, in Tynset, Hedmark County (Fig. 1 and Paus et al., 2006; Paus 2010). Features of the two lakes and their surroundings are listed in Table 1. In continental areas such as the study area, the birch-forest line roughly follows the 10 °C July isotherm (Odland, 1996). Both lakes lie in the low alpine zone characterized by lichen-dominated dwarf-shrub tundra. In Drivdalen, 2 km west of Finnsjøen (Fig. 1), birch-forests reach ca. 1100 m a.s.l., and pine-forests ca. 900 m a.s.l. The region including Finnsjøen is renowned for its well-developed and species-rich flora that includes plants with a so-called centric distribution in Scandinavia. More

details regarding environmental features of these sites are included in Paus et al. (2006, 2015) and Paus (2010).

3. Material and methods

We refer to Paus et al. (2006) and Paus (2010) for details on material and methods of the Flåfattjønna study. The Finnsjøen material and methods are described below.

3.1. Sampling and lithostratigraphy

The Finnsjøen lake sediments were cored at maximum water depth (14.7 m) from the ice-covered lake surface during winter. A 110-mm piston corer (Nesje, 1992) modified by A. Paus and J. Kusior (Dept. of Earth Science, Univ. of Bergen) was applied, which allowed us to use 6-m tubes and start sampling maximum 5 meters below the sediment surface. In Paus et al. (2015), results from the core section 1980-2195 cm below water surface were reported. The more detailed Holocene results presented in this paper, are based on the core section 1865-2040 cm depth below water surface showing distinctly laminated gyttja with numerous macrofossil and/or silty layers (Fig. 2). The analyzed sediments were described (Table 2) according to the method by Troels-Smith (1955). Sediments were cored in one continuous sequence. Hiati or correlated overlaps are absent in the core. However, during the XRF logging that requires length of sections less than 180 cm, one core section was cut one cm too long. Hence, 1 cm (2015-2014 cm depth below water surface) was removed from one core section. This 1 cm gap is shown as hiatus in Fig. 2.

3.2. Geochemical core logging

The loss-on-ignition (LOI) was measured in levels at 1-10 cm intervals in the studied core section. The sub-samples were dried overnight at 105 °C, weighed and ignited at 550 °C for 1 h. LOI was calculated as percentages of dry weight.

To document the sediment structure in the minerogenic part of the core, sediments were X-ray photographed using a Philips X-ray 130 kV instrument. The X-ray imagery was processed on a negative film, and thereafter transferred into a positive format using a digital camera. The resulting photos are found in Figs. 2 and 7.

The non-destructive ITRAX µXRF element core scanner from Cox Analytical Systems was applied to analyze variations in geochemical properties along the core surface as well as the colour- and the X-ray imaging. The core was scanned using a molybdenum (Mo) tube with a downcore resolution of 200 µm. The voltage and current were set to 35 kV and 50 mA, respectively, with a counting time of 10 s for each analytical step. The elements selected to represent downcore lithological variations are potassium (K) and calcium (Ca). In addition to elemental and colour scans of the core surface, a density graph was extracted from X-ray images and plotted versus depth with the same resolution like elemental analyses. Because X-rays penetrate through the core, they represent density and illustrate the overall layering that characterizes the sediment record.

3.3 Radiocarbon dating, varves and age-depth modelling

Eleven samples of terrestrial plant remains from the Finnsjøen sediments between 1810 and 2055 cm depth below water surface were AMS radiocarbon-dated (Table 3). All dates were reported as calibrated years BP (cal yrs. BP; present = AD 1950) based on the InCal13 calibration curve (Reimer et al. 2013). We converted the dates to calendar ages using CALIB 7.10 (Stuiver et al., 2017). The age-depth modelling (Fig. 3a) was obtained with the CLAM 2.2 R package (Blaauw, 2010) which recognized two outliers. The small variations in

sedimentation rates displayed in Fig. 3a most likely reflect dating inaccuracies. When estimating pollen accumulation rates (PAR) and plotting different sedimentary features versus age (Figs. 2, 4, 5, and 7), we used the linear sedimentation rate estimated by interpolating between the oldest and youngest dates.

When Figs. 2 and 7 were enlarged, a microscale pattern of the XRF density graph and the Ca and K curves appeared showing couplets of alternating maxima and minima. For the density graph, we counted ca. 3100 couplets in the analysed sediment sequence spanning ca. 3100 calibrated years, which indicates the presence of annual varves (see discussion in section 4.1). However, the density curve reflected a floating chronology with no fixed attachment points to the radiocarbon chronology (Fig. 3b). Only minor differences were noted between the two chronologies. We have chosen to use the radiocarbon chronology to date the onset of events and estimating the sedimentation rates. On the other hand, the varve chronology was used to estimate the duration of events.

3.4. Pollen

Material for pollen analysis was sampled at 0.5–15 cm intervals between 1865 and 2040 cm depth. The samples were treated with HF and acetolysed according to Fægri and Iversen (1989). We added *Lycopodium* tablets to the samples (1 cm^3) for estimates of concentration and pollen accumulation rates (PAR; Stockmarr, 1971). Identifications were based on Fægri and Iversen (1989), Moore et al. (1991), and Punt et al. (1976-1996) in combination with a reference collection of modern material at University of Bergen. *Betula nana* pollen was distinguished using the morphological criteria of Terasmäe (1951). The pollen diagrams (Figs. 4, 5, and 6) were drawn by the computer program CORE 2.0 (Kaland and Natvig, 1993). In the pollen percentage diagram (Fig. 6), the calculation basis (ΣP) comprised the terrestrial pollen taxa. For taxon X of aquatic plants (AQP) and spores, the calculation basis was ΣP+X. We used the computer program CANOCO 4.5 (ter Braak and Smilauer, 1997-

187 2002) for detecting and plotting ordination patterns in the terrestrial vegetation development.
188 The analysed data set included results from Lake Store Finnsjøen merged (using the option in
189 CORE 2.0) with pollen results from the same time interval (7600-10.700 cal yrs. BP) in
190 sediments of Lake Flåfattjønna, ca. 30 km east of Lake Finnsjøen (Paus, 2010; Paus et al.,
191 2006).
192
193 Palynological terrestrial richness (PR) was estimated by rarefaction analyses (program
194 RAREPOLL, Birks and Line, 1992) using the minimum sum of terrestrial microfossils (= 565)
195 as the statistical base ($E(T_{565})$). Intermediate levels of disturbance maximize richness by
196 preventing both dominance and extinction of species (Grime, 1973). In accordance with this,
197 the low estimated terrestrial PR $E(T_{565})$ for abundant tree pollen (AP) (Fig. 4) should indicate
198 closed forests, whereas local PR maxima indicated periods when the vegetation was positioned
199 close to and above the forest-line (e.g. Aario, 1940; Simonsen, 1980; Seppä, 1998; Grytnes,
200 2003). However, at Finnsjøen pine-pollen was not a local signal (see section. 5.2.). To estimate
201 local changes in palynological richness at Finnsjøen, we also estimated palynological richness
202 ($E(T_{102})$) by subtracting the dominant regional pine pollen from the statistical basis (Fig. 4).
203
204 *3.5. Biochemical characterisation*
205 C/N analyses: The lake sediments were freeze-dried for 48 hrs to remove all traces of water.
206 The freeze-dried samples were kept in a desiccator with 12M HCl (48 hours) to remove any
207 traces of carbonates present in the sediments (Hedges and Stern, 1984). Elemental C and N
208 were measured on a Perkin Elemental analyzer (2400 series II CHNS/O) for specific lake
209 samples together with certified standards (Jet Rock, Svalvard Rock). The reproducibility of
210 elemental analysis was ±10%.
211

Lipids: Plant waxes were extracted from ca. 1-4 g of freeze-dried sediment from selected intervals (see Fig. 2) with a mixture of dichloromethane and methanol (ratio of 9:1 by volume) by an automated solvent extraction (Dionex ASE 300). The total lipid extracts were injected into an Agilent 6890 gas chromatograph with a HP5-MS column (30 m× 0.25 mm internal diameter × 0.25 μm film). The oven temperature was kept constant at 35 °C for 6 minutes, increased to 300 °C at 5 °C min^{-1} and then held for 20 minutes. The chromatograph was coupled with an Agilent 5973 mass spectrometer and operated at 70 eV to scan the full range of charged particles from m/z 50 to 600 amu. High purity standards (S-4066) from Chiron (Trondheim, Norway) and deuterated compounds from Sigma-Aldrich (Munich, Germany) were used for quantification. The total input of higher odd *n*-alkane concentrations (*n*-C_{27}, C_{29} and C_{31}) was used to calculate the input of terrestrial plant waxes derived from higher plants. In addition, the ratio P_{aq} (Ficken et al. 2000) was calculated to estimate the input of waxes derived from in-lake algal production

$$P_{aq} = \frac{C_{23} + C_{25}}{C_{23} + C_{25} + C_{29} + C_{31}}$$

where C_n refers to *n*-alkane carbon chain length.

Glycerol dialkyl glycerol tetraether (GDGT): The total lipid extract of 11 of the Finnsjøen samples was re-dissolved in hexane/*iso*-propanol (99:1, v/v) and filtered using 0.45 μm PTFE filters. The branched and isoprenoidal GDGT distribution was analysed by high performance liquid chromatography/atmospheric pressure chemical ionisation – mass spectrometry (HPLC/APCI-MS) using a ThermoFisher Scientific Accela Quantum Access triple quadrupole MS. Normal phase separation was achieved using the method of Hopmans et al. (2016) that consists of two ultra-high performance liquid chromatography silica columns in

tandem. Injection volume was 15 µL from 300 µL. To increase the sensitivity and reproducibility, all analyses were performed using the selective ion monitoring mode (SIM) to detect specific ions (*m/z* 1302, 1300, 1298, 1296, 1294, 1292, 1050, 1048, 1046, 1036, 1034, 1032, 1022, 1020, 1018, 744, and 653).

The relative abundance of 6-methyl over 5-methyl br-GDGTs is expressed as the IR_{6me} ratio (De Jonge et al., 2013).

$$IR_{6me} = \frac{IIa' + IIb' + IIc' + IIIa' + IIIb' + IIIc'}{IIa + IIa' + IIb + IIb' + IIc + IIc' + IIIa + IIIa' + IIIb + IIIb' + IIIc + IIIc'}$$

In addition, the branched versus isoprenoidal tetraether (BIT) index (Hopmans et al., 2004) that reflects the relative abundance of the major bacterial br-GDGTs versus crenarchaeol, an iso-GDGT likely produced exclusively by *Thaumarchaeota* (Sinninghe Damsté et al., 2002), was also quantified

$$\mathrm{BIT} = \frac{(Ia + IIa + IIa' + IIIa + IIIa')}{(Ia + IIa + IIa' + IIIa + IIIa' + crenarchaeol)}$$

4. Results

4.1. Lithostratigraphy

The sedimentation rate appears approximately linear showing an average growth of 0.56 mm/ year (or 17.7 years/cm) in the studied time interval 10.700-7600 cal yrs. BP (Fig. 3a). The core section 1865-2040 cm below the water surface consists of distinctly laminated to sub-laminated gyttja as indicated by the high-resolution colour scan and the density graph plot. The lamina observed by eye (Figs. 2 and 7) are normally 0.5-0.6 mm thick and occur as greyish silty horizons or as darker layers of distinct concentrations (amount) of macrofossils. The variability

262 in the density graph also shows the laminated structure of the core confirming that the
263 lamination is not only preserved in the top layer of the core, but is the structure of the entire
264 core. Down-core density is plotted versus the number of electrons penetrating the core section
265 for every 200 μm. The lower the cps number is, the higher the density. And the higher sediment
266 density is, the higher minerogenic content in the core. The shift from minerogenic sediments to
267 an increasing amount of biogenic components is clearly shown at ca. 10350 cal yrs. BP. The
268 shift at 9800 cal yrs. BP to lower sediment density (higher cps) reflects transfer to a period with
269 increased biogenic production and content. These depositional conditions dominated by higher
270 biogenic production, characterise the period studied in this core. It is punctuated by short
271 periods of increased minerogenic content, composed of higher density and/or lower
272 productivity, centred around 9650, 9340 and 8200 cal yrs. BP (Figs. 2 and 7). Similarly, the
273 relative concentration of potassium (K) and calcium (Ca) reflects the lithological variability
274 with similar amplitude as expressed in the density graph. These lithological variations around
275 the postulated cool periods are consistent with colour imaging indicating distinct shifts in
276 colour. Notably, the lamina appear coarser and thicker than the warm periods (Figs 2 and 7).
277 Because K and Ca represent particles from the local bedrock, the variability measured reflects
278 shifts in allochtonous contributions. The major increases of K and Ca around cooling periods
279 is centred around 9650 and 8200 cal yrs. BP and illustrates the sensitivity of this parameter to
280 local environmental changes.

281 The lithostratigraphy also shows microscale laminations superimposed on the laminations
282 observed by eye. Both for sediment density and the elements K and Ca there are densely shifting
283 values where maxima alternate with minima forming couplets (Figs. 2 and 7). We counted 3117
284 density couplets over the 3100 calibrated years spanned by the analysed Finnsjøen sediments.
285 This strongly points to the deposition of annual varves in Finnsjøen, here reported for the first
286 time in Norway. The density maxima (i.e. low cps) reflect increased allochtonous minerogenic
287 input during the thawing in spring/early summer, whereas the density minima (i.e. high cps)

represent autochtonous organic production during summers (consistent with lower C/N and terrestrial organic matter input albeit representing low-resolution measurements). Hence, the varve origin appears as a mixture of clastic and biogenic factors (Zolitschka et al., 2015).

The clear-cut changes in K and Ca concentrations at the lower boundary of the 9.7 and the 8.2 cooling events are interpreted to represent gaps of 1.1–1.5 cm of the lake record due to climate influenced erosion of the underlying laminated units. These estimates are based on the counting and thickness estimates of lamina compared with the age model (Fig. 3a). The gaps are calculated to represent a removal of maximum 12 years of sediments at the beginning of the 9.7 event and maximum 20 years of sediments at the beginning of the 8.2 event. Obviously, this reflects a source of error for establishing a reliable varve chronology.

4.2. Pollen results and statistical analysis

We identified 47 terrestrial taxa in 47 levels of the Finnsjøen sediment-section. The pollen sum of terrestrial taxa analysed per sample varied between 535 and 2066 (mean ΣP: 1035). Seven local pollen assemblage zones were defined by visual inspection (Figs. 2, 5 and 6, Table 4). In five PAZ (S-2 to S-6), pine dominates showing values of 40-90% ΣP. During this period of pine maximum, there are two distinct and short-lasting pine minima of 40-50% ΣP (PAZ S-3 and S-5). At the same time, *Betula, Juniperus* and algae show percentage maxima.

The merged data set from lakes Finnsjøen and Flåfattjønna was subjected to a DCA ordination that showed a gradient length of 1.70 SD. This suggested linear response curves. Hence, we chose PCA as an ordination technique. A preliminary PCA including the dominant and entirely regionally represented *Pinus* (see section 5.2.), condensed scatter plots, and axis 1 captured 62% of the variation in the data. To reduce the influence of pine and enhance the influence of local features, pine was included as passive in the PCA (Figs. 8 and 9). Palynological richness (PR) and LOI were added as environmental variables during the

statistical assessment. In Fig. 8, the light-demanding pioneers are concentrated to the left with medium to low axis 2 values, along with PR. Deciduous trees (e.g. *Ulmus, Corylus*) and herbs (e.g. *Valeriana, Geranium*) on fertile soils are situated to the right and/or at high axis 2 values. *Pinus* and LOI occur to the extreme right.

4.3. Biochemical results

C/N ratio varies between 12-20 indicating inputs of lacustrine algal production and higher plants from the catchment typical of lacustrine environments (Das et al., 2008). Higher values coincide with the onset of the cold 9.7 and 8.2 events due to soil erosion and increased outwash of nutrients, before it declines with the intensification of colder temperatures. C/N gradually increases after the cold periods. This transition is most evident after the 8.2 event.

n-Alkane concentrations increase core upwards with inflection points coinciding with the 9.7 and 8.2 cooling events (Fig. 2), interpreted as terrestrial organic matter and aquatic input. A lower P_{aq} ratio suggests less algal productivity. The percentage of terrestrial organic matter (mainly plant waxes) declines sharply by nearly 20% after the onset of the cold events and recovers again after climate ameliorates and vegetation recovers in the catchment. The increase of terrestrial organic matter is larger during the post-9.7 warming than during the recovery after the 8.2 event.

Glycerol dialkyl glycerol tetraethers (GDGTs) are abundant biomarkers in most types of natural archives (Schouten et al., 2000; Schouten et al., 2013). Two types of main GDGTs are recognized; Archaea synthesize isoprenoidal (iso-GDGTs), whereas bacteria synthesize branched (br-GDGTs) compounds. In general, br-GDGTs are more abundant in terrestrial settings, whereas iso-GDGTs are more abundant in sediments from large lakes and marine environments (Hopmans et al., 2004). Iso-GDGTs can have between 0 and 8 cyclopentane rings, whereas crenarchaeol has four cyclopentane and one cyclohexane ring (De Rosa and

Gambacorta, 1988; Schouten et al., 2000; Sinninghe Damsté et al., 2002; Schouten et al., 2013). br-GDGTs can have between 0 and 2 cyclopentane rings and/or between 0 and 2 additional methyl groups at either the C5 and C6 position (De Jonge et al., 2013; Schouten et al., 2000, 2013; Sinninghe Damsté et al., 2000).

In mineral soils, peat, and lake sediments, the degree of methylation of br-GDGTs is correlated with mean annual air temperature (MAT), while the degree of cyclization of br-GDGTs and the relative abundance of 6-methyl br-GDGTs over 5-methyl br-GDGTs is correlated with the pH (e.g., Weijers et al., 2007; Loomis et al., 2012; De Jonge et al., 2014; Naafs et al., 2017; Russell et al., 2018).

In all 11 samples from Finnsjøen, taken between 2022 and 1870 cm below water depth, GDGTs were present in abundance. The GDGT distribution was dominated by bacterial br-GDGTs over archaeal iso-GDGTs. The dominant archaeal lipid was iso-GDGT-0 with a relative abundance over iso-GDGT-1, -2, and -3 above 90%. Crenarchaeol was present in low abundance and the BIT index, reflecting the ratio between br-GDGTs and crenarchaeol, varied between 0.98 and 1.00. The br-GDGTs were dominated by acyclic 5-methyl homologues Ia, IIa, and IIIa with the latter being the most abundant compound with a relative abundance over all br-GDGTs of ~ 30%. In all samples, 5-methyl br-GDGTs were the most abundant, but 6-methyl br-GDGTs were also present. The IR_{6me} ratio, reflecting the ratio between 6- and 5-methyl br-GDGTs, ranged from 0.3 to 0.4.

The dominance of br-GDGT over iso-GDGTs, the small size of the lake, as well as the broader biomarker distribution (see above) suggests that the majority of GDGTs are derived from the surrounding soils. As such we used the global mineral-soil based calibration to convert the br-GDGT distributions into temperature and pH estimates (De Jonge et al., 2014).

$$MAT_{mr}\ (^{O}C) = 7.17 + 17.1 \times \{Ia\} + 25.9 \times \{Ib\} + 3.44 \times \{Ic\} - 28.6 \times \{IIa\}\ (\text{RMSE} = 0.46\ ^{o}C)$$

$$pH = 7.15 + 1.59 \times CBT' \quad (\text{RMSE} = 0.52)$$

$$CBT' = \log \frac{(Ic + IIa' + IIb' + IIc' + IIIa' + IIIb' + IIIc')}{(Ia + IIa + IIIa)}$$

The MAT_{mr}-based temperatures range between 3 and 6 ± 4.6 ºC. Temperatures gradually decrease along the core with highest temperatures recorded in the oldest samples. The pH was relatively constant around 6.5 and mimics the temperature decline with slightly higher pH values in the oldest samples (Fig. 2).

5. Discussion

5.1. Background climate

The low-resolution biomarker data based on *n*-alkanes and br-GDGT provides complementary information about the organic matter sources and how the changes were driven by climate fluctuations.

The br-GDGT based terrestrial temperatures (MAT_{mr}) from Finnsjøen (Fig. 2) provide a general context of background climate in the region on which the "Bond"-events are superimposed. We explicitly assume that 1) br-GDGTs in the mineral soils surrounding the lake are the main source of these compounds accumulating in the lake sediments, and 2) br-GDGT distribution is biased towards the warmer season. It is hard to confirm these assumptions, but given that we do not detect the novel hexamethylated GDGT only known from lacustrine production (Weber et al., 2015), the small size of the lake, abundant presence of higher plant waxes and elevated C/N values, it is likely that most of the organic matter in the lake sediments is not derived from *in situ* production in the lake. At present, the region

395 experiences temperatures well below freezing during winter months with average
396 temperatures in January around -11.5 ºC (Table 1). Temperatures are on average 7.5 ºC in
397 July. It is not clear whether br-GDGTs in soils that experience <0 ºC temperatures during part
398 of the year are predominantly produced during the warmer season (Peterse et al., 2009;
399 Weijers et al., 2011; Deng et al., 2016), but as bacterial growth is temperature dependent, it is
400 likely that production of br-GDGTs in top soils is dominated by production when
401 temperatures are above freezing, before being washed into the lake. The reconstructed
402 temperatures for the early Holocene between 3 and 6 ± 4.6 ºC are 5 to 8 ºC higher than
403 present-day annual mean temperatures of -2.5 ºC, further supporting a bias in br-GDGT
404 production to periods when temperatures are above freezing. For comparison, the average of
405 mean monthly temperatures above zero is today estimated to 3.5 to 4 ºC at the altitude of
406 Finnsjøen. The temperature evolution with ~2 ºC higher MAT_{mr} around 10.000 cal yrs. BP
407 compared to 8000 cal yrs. BP, follows the local summer insolation pattern (Fig. 2), providing
408 additional evidence that the record is biased towards the warm season. Thus, it does not
409 represent the annual mean temperatures. Our data supports the hypothesis that the Holocene
410 thermal maximum (HTM) in Scandinavia occurred during the early Holocene, and may have
411 occurred earlier than the pine maximum in this region.
412
413 The MAT_{mr} calibration error of ± 4.6 ºC and sample resolution prevent the identification of
414 Bond-events in the temperature record. However, MAT_{mr} does provide information about the
415 regional background climate, which was a few degrees C warmer than at present. This is
416 consistent with palaeobotanical records from southern Scandes Mountains (Kullman, 2013;
417 Paus, 2013; Paus & Haugland, 2017).
418
419 *5.2. Regional pine pollen*
420 The period in focus includes the Early Holocene pine maximum that is distinctly displayed in
421 pollen diagrams from alpine areas in South-Scandinavia (e.g. Bergman et al., 2005; Bjune,

2005; Gunnarsdottir, 1996; Velle et al., 2005, Segerström and Stedingk, 2003). During this pine maximum, numerous megafossils show that the pine-forests reached their maximum elevation in south-Scandinavia (Selsing, 1998; Kullman, 2013; Paus and Haugland, 2017). These pine forests perhaps never reached much higher than 1105-1110 m a.s.l. in the study area because no megafossils are found above this elevation (Paus, 2010; Paus et al., 2011). According to Paus & Haugland (2017), pine-forests did not reach more than ca. 250 m higher than present forests during the pine maximum. This would imply an early Holocene pine forest-line at ca. 1150 m a.s.l. at Dovre, which is ca. 100 m lower than the altitude of Finnsjøen. Pollen and macrofossil data from Råtåsjøen (1169 m a.s.l.), ca. 16 km SSE of Finnsjøen, supports this conclusion (Velle et al. 2005).

On the other hand, the pine sedaDNA (Paus et al., 2015), the extremely high pine PAR (45 10^3 grains cm^{-2} a^{-1}), and the high pine pollen percentages (90 % ΣP) in sediments of Finnsjøen (1260 m a.s.l.) could contradict this conclusion. We regard these evidences of local pine forests as doubtful based on the following arguments. Pine sedaDNA was only found in one core-interval (Paus et al., 2015) which could reflect long-distance transport of pine remains or single specimens of low-growing "Krumholz" pine that are currently found up to 1200 m a.s.l. at Dovre. The PAR values are ca. 40 times higher than the threshold for indicating local pine forests (Jensen et al.; 2007; Seppä and Hicks, 2006) and reflect extreme sediment focusing (Davis et al., 1984; see discussion in Paus et al., 2015). Lastly, lowland hillsides in Drivdalen (Fig. 1) where tree-birch and pine grow today, would have been important sources for long-distance pollen. Such pollen could be dominant when local pollen production was low. Moreover, it is macrofossils of *Betula pubescens* and not pine that are found in the Finnsjøen sediments (Table 3) indicating presence of birch-forests in adjacent areas. The pine derived pollen is nevertheless dominant in the lacustrine record. Perhaps the birch-forests were open and had low pollen-production. Hence, the representation of long-distance pine pollen was enhanced in the sedimentary record. It is well known that pine is represented by

dominant long-distance transport in other pollen based studies from the Arctic-Alpine regions (Aario, 1940; Gajewski, 1995; Paus, 2000). With these interpretative constraints on the pine pollen signal, we reconstruct the following local vegetation and climate development for the Finnsjøen area.

5.3. General trends of local vegetation development

The PCA ordination (Figs. 8, 9) roughly displays gradients of vegetation density/soil thickness increasing towards the right (axis 1) and soil fertility increasing upwards (axis 2). At Finnsjøen, pollen from *Pinus* and the warmth-demanding *Corylus, Ulmus*, and *Quercus* shows the strong influence of long-distance pollen transport. Nevertheless, local successions can be distinguished. Species-diverse pioneer vegetation on shallow soils developed (PAZ S-1; lower left in Figs. 8, 9), and is followed by forests with *Betula pubescens, Populus tremula*, and (from 9300 cal yrs. BP) *Alnus incana* on more organic-rich soils (PAZ S-2 to S-6). Thereafter, tall-herb *Betula/Sorbus/Alnus* forests with e.g. *Valeriana, Geranium, Filipendula*, and *Urtica*, developed on the fertile soils in protected sites locally, whereas dwarf-shrub heaths expanded on wind-exposed ridges (PAZ S-7).

Within the same period (7600-10.700 cal yrs. BP), the local development at Flåfattjønna followed a similar pattern (Paus, 2010), but deviated chronologically in some successional stages. First, Flåfattjønna was deglaciated more than 800 years later than Finnsjøen (Paus et al., 2015), and therefore showed a lagged succession by a delay in leaching of soil minerals into the lake. Fig. 9 shows that pioneer plant communities on unweathered mineral-soils (PAZ F-2) developed ca. 10.700 cal yrs. BP at Flåfattjønna; a successional stage that was reached earlier at Finnsjøen (Paus et al., 2015). However, even if weathering and leaching of soils started just after local deglaciation, soil pH was still high at Finnsjøen in PAZ S-1 (Fig. 2). Second, even if pine-forests thrived at Flåfattjønna (1110 m a.s.l.) and did not at Finnsjøen (1260 m a.s.l.), the pollen record showed maximum pine values for a longer period at

Finnsjøen (ca 10.000 – 8000 cal yrs. BP) compared to Flåfattjønna (9700 – 8500 cal yrs. BP; Fig. 4). It is likely that Drivdalen (2 km west of Finnsjøen and 700 m a.s.l.; Fig. 1), where temperatures allowed pine to grow for a longer period than at higher elevations, was an important contributor to the regional pollen representation at Finnsjøen. This would result in a stronger and longer-lasting percentage signal at the high-altitude Finnsjøen with vegetation of lower local pollen production than at Flåfattjønna (cf. Aario, 1940; Ertl et al., 2012).

During the pine maximum, when Finnsjøen was situated close to the upper birch-forest ecotone, and Flåfattjønna was situated close the upper pine-forest ecotone, the two distinct episodes of reduced pine percentages occur around 9700 cal yrs. BP and 8400-8200 cal yrs. BP at both Finnsjøen and Flåfattjønna (Fig. 4).

5.4. The 9.7 cold event – Erdalen event 2

Around 9700-9600 cal yrs. BP in the Finnsjøen sediments, pine percentages, pine PAR, and LOI (Figs. 2, 4, 5 and 6) reach short-lasting minima, K and Ca element intensity and X-ray density (Fig. 2) reflect increased soil erosion and outwash resulting in increased lamina thickness, whereas *n*-alkanes show lowered input of both terrestrial organic matter and aquatic homologs (Fig. 2). The short-lasting C/N maximum is interpreted to reflect erosion and outwash of terrestrial organic matter, whereas declining C/N values show that colder conditions reduced terrestrial input more than the aquatic production (cf. alkanes of terrestrial organic matter *vs.* P_{aq}). The first part of the subsequent C/N rise reflects lower aquatic production, whereas the later rise shows a warming that increased the terrestrial input more than the aquatic production according to the *n*-alkane trends.

In PAZ S-3 of the Finnsjøen pollen diagram, constituting the three-level pine percentage minimum (Fig. 6), PAR values of *Betula*, *Juniperus*, and *Salix* show little change from the previous S-2 (Fig. 5). Hence, their S-3 percentage maxima reflect the reduction of pine

503 entirely represented by regional/long-distance pollen (see section 5.2.). In addition, after
504 removing regional pine from the calculation basis, palynological richness shows no distinct
505 changes (Fig. 4). However, PCA with pine removed from the data set, shows that the local S-
506 3 vegetation returned towards previous pioneer stages of S-1 (Fig. 9). Altogether, the
507 stratigraphical trends indicate the 9.7 changes as a cold event that influenced lacustrine and
508 terrestrial productivity. However, the GDGT temperature estimates show no distinct changes
509 (see section 5.1).
510
511 The onset of the 9.7 cold event is signaled by both regional (i.e. decline in pine) and local
512 (e.g. Ca and C/N increase) parameters. The floating varve chronology (see section 4.1)
513 suggests that LOI decreased ca. 10 years later than pine. This delayed LOI decrease might
514 reflect the time needed to erode top soil within the lake's catchment. The soil-independent
515 algae (cf. *Pediastrum*) took advantage of nutrients washed out during the cold event. They
516 flourished around the same time as regional pine abruptly increased (Figs 2, 5 and 6) both
517 trends support the onset of climate warming during this period. Local vegetation regrowth and
518 soil formation, shown by increasing LOI, lagged climate amelioration by 10-15 years
519 according to the varve chronology. The upper boundary of the dark eroded layer occurs when
520 LOI reached pre-9.7 values.
521
522 According to the floating varve chronology (Figs. 3b, 7), the impact of the 9.7 cold event
523 lasted ca. 56-58 years. Increased soil erosion and outwash during the event seem to have
524 increased varve thickness above the average sedimentation rate of 0.56 mm/yr to a rate of ca.
525 0.77 mm/yr. Accordingly, the influence on regional pine lasted for ca. 56-58 years before pine
526 pollen production recovered. Missing sediments from this section could add maximum 12
527 years to the duration of the 9.7 impact (see section 4.1). Most probably, a period of about 60-
528 70 years is too short for pine forests to recover totally after being decimated by very cold
529 conditions (cf. Kullman, 1986, 2005). We think that the distinct pine oscillation reflects a

multi-decadal cold period whereby pine survived, but experienced reduced pollen production. According to Dahl et al. (2002), the 9.7 glacial advance at Jostedalsbreen, ca. 150 km WSW of Finnsjøen reflects a cooling of at least 1°C. This would have reduced the pine pollen production by a similar magnitude as displayed in the Finnsjøen pollen diagram (cf. Hicks, 2006).

Notably, at Flåfattjønna, an erosion layer distinctly reflects the 9.7 event. This layer including pine seeds and needles shows that pine pollen percentages and LOI decrease after the decline in pine PAR (Paus, 2010). The pine percentage maximum at the pine PAR minimum (Fig. 4) reflects outwash of soils containing remains of local pine (pollen and macrofossils) when regional and local total pollen production was reduced (Paus, 2010). In addition, at Flåfattjønna, PCA indicates regression of local vegetation towards pioneer stages during the 9.7 event (Fig. 9).

According to the radiocarbon chronology (Fig. 3a), this cold event occurred ca. 9605-9675 cal yrs. BP interpolated (Figs. 2), but the varves suggest the duration to be around 56-58 years (Fig. 7). At Flåfattjønna, the cold event is predicted based on fewer ^{14}C dates (Fig. 4). This low-resolution and inaccurate chronology dates the event to ca. 9500-9700 cal yrs. BP (Paus, 2010).

5.5. The 9.3 cold event

At both Flåfattjønna and Finnsjøen, the post-9.7 warming initiated a vegetation closure reaching the Holocene maximum according to total PAR (Fig. 4). At Finnsjøen, the vegetation closure strongly reduced palynological richness. This warming also initiated the rapid establishment of broad pine-forest belts in mid-Scandinavia, reflecting the July mean Holocene maximum (Paus and Haugland, 2017). Shortly thereafter, during the first half in Finnsjøen PAZ S-4 (Fig. 6), a small-scale cooling parallel to the 9.7 event is detected around

9300 cal yrs. BP (at 1963 cm depth, see also table 2), showing a minimum in sediment density and decreasing pine, and a delayed increase in freshwater algae (*Pediastrum, Botryococcus;* Figs. 2, 6). Furthermore, local vegetation became more open shown by decreasing total PAR (Fig. 5), increasing light-demanding shrubs and dwarf-shrubs (Fig. 6), and an increase in long-distance pollen (cf. *Corylus*). We think these changes reflect a climate cooling, though its local effect was less extensive than the 9.7 impact at Finnsjøen. As for the 9.7 event, the delayed increase in freshwater algae could indicate the warming following the short-lasting cold event. The 9.3 cooling reflects the collapse of the Laurentide Ice Sheet (Yu et al., 2010; Gavin et al., 2011) with distinct impacts in Canada (Gavin et al., 2011), Greenland (Young et al. 2013), Iceland (Brynjolfson et al., 2015), and further south at the Iberian Peninsula (Burjachs et al., 2016; Iriarte-Chiapusso et al., 2016). The 9.3 event is also recorded in the Greenland ice-cores (Vinther et al., 2009; Rasmussen et al., 2014). Furthermore, signals of the 9.3 south of Svalbard are weak (Werner et al., 2016). This, in line with the scarcity of Fennoscandian 9.3 records in eastern Europe and its limited impact at Finnsjøen, indicate that the 9.3 cooling had its main influence in western and southern coastal Europe.

In Finnsjøen, the 9.7 event (Erdalen 2) and 9.3 event are recorded as two distinct separate events. We therefore emphasize that the 9.7 event, which seems to have a Fennoscandian origin, i.e. the drainage of the Baltic Ancylus Lake (Nesje et al., 2004), is not formally a "Bond" event, and must therefore not be confused with the 10.3 or 9.3 "Bond" events of North Atlantic Ocean origin (Bond et al., 1997, 2001).

5.6. The 8.2 cold event – Finse event

At Finnsjøen, the post-9.3 changes with slight increase in vegetation density (Fig. 5), favored the moisture-demanding *Alnus* to expand within the area. Thereafter, stable records of vegetation and other parameters indicate a period of stable climate until ca. 8420 cal yrs. BP at the PAZ S-4/S-5 transition (Fig. 6), where colder temperatures are signaled. Here, pine

584 percentages and PAR values decrease, probably due to a decline in summer temperatures that
585 decreased regional pollen production (Paus and Haugland, 2017). The slightly later increase
586 in tree-birch and alder PAR values (Fig. 5) could in addition reflect the lowering of vegetation
587 belts within the region and the descent of the more warmth-demanding pine-forest. The rise in
588 *Alnus* PAR indicates the presence of more moist and fertile soils in the region, whereas
589 macrofossils (Table 3) show the local presence of birch-forests. The increase in juniper (Figs.
590 5 and 6) reflects more open vegetation locally, and PCA (Fig. 9) shows the recurrence
591 towards more pioneer vegetation. The decreasing LOI and sediment density in the last part of
592 S-5 (Fig. 2) point to increased soil erosion and outwash.
593
594 Around the S-5/S-6 transition at ca. 8225 cal yrs. BP, pollen data indicate harsher conditions
595 showing a maximum in palynological richness (Fig. 4) and representation of pioneers
596 (*Saxifraga oppositifolia* type, *Empetrum*) in a short period with low total PAR between the
597 earlier birch and alder decrease and the later pine rise in the pollen diagrams (Figs. 5 and 6).
598 Apparently, the birch-forest ecotone was lowered which displaced the local area towards the
599 tundra vegetation zone. This opening of local vegetation occurs at the same time when
600 erosion of terrestrial organic matter intensified, and further supported by the short-lasting
601 maximum in C/N-ratio (Fig. 2). Thereafter, the deposition of a dark minerogenic layer (Figs.
602 2 and 7, Table 2) is initiated showing minimum sediment density, K, Ca, and LOI. This
603 reflects maximum erosion and outwash due to deteriorating climate conditions. At the same
604 time, an increase in pine in early S-6 (Figs. 5 and 6) reflects expanding regional pine-forests
605 and/or increasing pine-pollen production. Both alternatives reflect warmer conditions during
606 summer. A warmer lake could also be indicated by decreasing C/N values due to increased
607 algal growth. This apparently contrasting evidence of climate points to the 8.2 weakening of
608 the Atlantic current (Daley et al., 2011; Holmes et al., 2016) that resulted in an increased
609 continental climate and enhanced amplitude of seasonal temperatures and involved at least
610 colder winters (Alley and Ágústdóttir, 2005). Hence, even if widespread local areas were

exposed to maximum freezing/thawing and erosion due to a period of less snow and more wind during colder winters, summers became warm enough to allow regional pine to expand and/or increase its pollen production.

The bio- and litho-stratigraphy in PAZ S-5 and S-6 shows a two-step climate deterioration. The first of moderate impact is mainly signaled by the biostratigraphy at the PAZ S-4/S-5 transition, from ca. 8420 cal yrs. BP, whereas the second and strongest period is mainly reflected by geochemistry and a dark erosional layer that deposited from ca. 8225 cal yrs. BP close to the PAZ S-5/S-6 transition. The varve chronology suggests that this dark layer spans a period of ca. 38 years (Fig. 7). Probably, missing sediments could add maximum 20 years to this duration (see section 4.1.), which indicates that climate deterioration intensified ca. 8245 cal yrs. BP or a few years later. This coincides approximately with minimum $\delta^{18}O$-derived temperatures in the Greenland ice core (Fig. 2).

According to Rasmussen et al. (2014), the 8.2 event started ca. 8250 cal yrs. BP which is close to the estimated age of PAZ S-5/S-6 transition and the deposition of the erosion layer. It is likely these abrupt stratigraphical changes signal the sudden outburst of Lake Agassiz and the strong meltwater pulse into the North Atlantic that caused colder, drier and windier conditions globally (Alley et al., 1997; Alley and Áugústdóttir, 2005). Most probably, the moderate changes ca. 8420 cal yrs. BP reflects a longer-term cooling upon which the 8.2 event is superimposed (Rohling and Pälike, 2005).

A third phase, representing a recovery phase, from ca. 8175 to 8050 cal yrs. BP, shows increasing sediment density, K content, LOI, and total PAR (Figs. 2 and 5), which reflects stabilizing soils and re-development of vegetation cover. This long-lasting re-establishment phase of more than hundred years indicates that conditions gradually improved. The exposed position of Finnsjøen could partly explain the slow regrowth locally. On the other hand, the

638 short-lasting algal-maximum ca. 8100 cal yrs. BP could indicate further warming that
639 differentiates an older and still rather cold and unfavorable phase from a younger and warmer
640 phase. In total, 370 years elapsed extending from ca. 8420 to 8050 cal yrs. BP, before the
641 Finnsjøen vegetation totally recovered from the 8.2 impact.
642
643 At Flåfattjønna, the low-resolution chronology displays a 400 years local response (ca. 8550
644 to 8150 cal yrs. BP; Paus, 2010) to the 8.2 (*sensu lato*) impact appearing in a two-step moist-
645 dry pattern. However, both steps were regarded as cold periods (Paus, 2010). Similar two-step
646 patterns are a wide-spread phenomenon as reported by other researchers (e.g. Nesje and Dahl,
647 2001; Ojala et al., 2008; Rasmussen et al., 2008; Filoc et al. 2017). According to Rasmussen
648 et al. (2014), the impact of the freshwater impulse into the North Atlantic lasted ca. 150 years
649 (ca 8250 to 8090 cal yrs. BP), but terrestrial sites show longer-lasting responses of varying
650 lengths (Filoc et al., 2017). Although a varying degree of dating precision must be considered,
651 one must expect that the duration of vegetation responses to the same impact depends on both
652 the geographical position (e.g. N-S, E-W, distance from coast) and distance from ecotones.
653 Study sites at ecotonal positions, i.e. being less resilient to disturbance (such as the Finnsjøen
654 and Flåfattjønna sites), seem to show long-lasting responses to the 8.2 event. Such sites
655 probably were more vulnerable to the background climate variations such as the 8.2 precursor
656 (Rohling and Pälike, 2005). Most probably, ecotonal sites also show a slow recovery after
657 cold events.
658
659 *5.7. The 9.7 and 8.2 events compared*
660 Both at Flåfattjønna and Finnsjøen, the impact of the 8.2 event *sensu lato* (ca 370-400 years)
661 lasted longer than the influence from the 9.7 cooling event (60 to < 200 years). At
662 Flåfattjønna, the distinct PCA responses (Figs. 4 and 9a) show that the 8.2 event had a
663 stronger impact on local vegetation than the 9.7 event. At Finnsjøen, with a better
664 stratigraphic time resolution than Flåfattjønna, the strength of the two events could be

665 reflected by increased sedimentation rate of their erosional layers. According to the varve
666 chronology, the sedimentation rate of the 9.7 erosional layer is ~ 4.4 cm during 56-58 years
667 (0.79-0.76 mm/yr), whereas the 8.2 erosional layer show a sedimentation rate of ~2.8 cm
668 during 38 years (0.74 mm/yr). On the other hand, the 8.2 erosion occurred at a higher
669 successional stage with denser vegetation on more mature soils (Fig. 9), i.e. when local
670 vegetation was at a distance from ecotones and more resilient to disturbance. In spite of that,
671 erosion during the 8.2 event shows similar values as during the 9.7 cold spell. Hence, the 8.2
672 cold event appears to have been stronger than the 9.7 cold event in the Finnsjøen area, and
673 probably also over larger regions as signals of the 9.7 event are scarce.
674
675 To estimate patterns of impact, it would have been of interest to compare these results with
676 studies from a wider area. To the best of our knowledge, other pollen records of the 9.7 event
677 in Scandinavia are absent, whereas pollen signals of the 8.2 event are sparse in alpine south
678 Norway.
679
680 At Topptjønna, 1.7 km south of Finnsjøen, the 8.2 event also shows a moist-dry two-step
681 pattern, but the study was carried out with a much lower time resolution than at Finnsjøen
682 (Paus et al., 2011). In Jotunheimen, ca. 110 km SW of Finnsjøen, the 8.2 event appears as a
683 short reduction in pine pollen (Barnett et al. 2001; Gunnarsdottir, 1996). The Leirdalen site of
684 Barnett et al. (2001) shows a strong pine oscillation from 90 % to 45 % and back to 90 %,
685 lasting less than 80 years. Pine stomata show the presence of pine during the pine pollen
686 minimum. Otherwise, the pollen percentages of *Betula, Salix* and herbs increased. This has
687 been interpreted as a short-lasting cold event that affected pine pollen production but not the
688 vegetative growth locally (Hicks, 2006). The similar pollen-stratigraphical patterns during the
689 short-lasting Finnsjøen 9.7 event have been interpreted similarly (see section 5.4). During the
690 9.7 event, Finnsjøen was lying in open birch-forests well above the pine-forest line (see
691 section 5.2.), whereas the Leirdalen site (920 m a.s.l.) was situated in closed pine-forests

692 during the 8.2 event and far below the upper pine-forest ecotone. Even being situated at
693 opposite sides of an ecotone, the border between pine-forest and birch-forest, the two sites
694 showed similar pollen responses to the weaker 9.7 and the stronger 8.2 cooling, respectively.
695 This demonstrates how vegetation response is determined by both the impact and the ecotonal
696 position of the vegetation cover (cf. Smith, 1965; Fægri and Iversen, 1989)
697
698 **6. Conclusions**
699
700 • The sediments of Finnsjøen and Flåfattjønna show exceptionally strong stratigraphical
701 signals of the 9.7 and 8.2 cooling events. The positions of these sites close to ecotones
702 (vegetation borders) were decisive in reducing their resilience against climate
703 fluctuations.
704 • At Finnsjøen and Flåfattjønna, the impact of the 8.2 event was stronger than the 9.7
705 event.
706 • During the abrupt 9.7 cooling event at Finnsjøen, pine pollen percentages became
707 halved and re-established in less than 60 years indicating that pine pollen production
708 was severely reduced due to lower summer temperatures.
709 • At Finnsjøen, the 8.2 event *sensu lato* (ca. 8420 – 8050 cal yrs. BP) can be divided
710 into a precursor lasting ca. 195 years, an erosional phase lasting ca. 50 years, and a
711 recovery phase lasting ca. 125 years. At the onset of the erosional phase, summer
712 temperatures increased.
713 • In the Finnsjøen sediments, weak signals indicate a cold spell at 9300 cal yrs. BP.
714 Both the 8.2 and 9.3 events reflect collapses of the Laurentide Ice Sheet and represent
715 two of the global "Bond" events. The 9.7 event most probably reflects the drainage of
716 the Baltic Ancylus Lake hat had restricted regional impact.

- The XRF sediment density graph documents annual varves throughout the studied Finnsjøen sediments.
- br-GDGT-based temperatures are biased towards warmer seasons and indicate gradual cooling throughout the Early Holocene, following local summer insolation.
- C/N ratios indicate input of lacustrine algal production and higher plant matter from the catchment area.
- Higher C/N values coincide with the onset of cold events and declines with its intensification; C/N increases again after the cold period.
- Input of terrestrial organic matter (plant waxes) decreases during cold conditions followed by its steady increase afterwards.

Acknowledgements

We thank Espen Paus, Erling Straalberg, and Ståle Samuelshaug for help during coring. The ITRAX μXRF core scanner system at the EARTHLAB, Department of Earth Science, University of Bergen, was used for elemental analyses, color and x-ray image scanning of the core. We also want to thank two anonymous reviewers for valuable comments which significantly improved the manuscript.

Funding sources

This work was financially supported by the Olaf Grolle-Olsen and Meltzer University Foundations

References

Aario, L., 1940. Waldgrenzen und subrezente Pollenspektern in Petsamo Lappland. Annales *Academia Scientiarum Fennica* A 54 (8), 1-120.

743 Alley, R.B., Mayewski, P.A., Sowers, T., Stuiver, M., Taylor, K.C. and Clark, P.U., 1997.
744 Holocene climatic instability: A prominent, widespread event 8200 yr ago. *Geology*
745 25(6), 483–486.
746 Alley, B., Ágústsdóttir, A.M., 2005. The 8k event: cause and consequences of a major
747 Holocene abrupt climate change. *Quaternary Science Reviews* 24, 1123-1149,
748 doi:10.1016/j.quascirev.2004.12.004.
749 Andersen, C., Koc, N., Moros, M., 2004. A highly unstable Holocene climate in the subpolar
750 North Atlantic: evidence from diatoms *Quaternary Science Reviews* 23, 2155-2166.
751 doi:10.1016/j.quascirev.2004.08.004.
752 Bakke, J., Dahl, S.O., Nesje, A., 2005. Lateglacial and early Holocene palaeoclimatic
753 reconstruction based on glacier fluctuations and equilibrium-line altitudes at northern
754 Folgefonna, Hardanger, western Norway. *Journal of Quaternary Science* 20, 279–
755 298, doi:10.1002/jqs.893.
756 Bergman, J., Hammarlund, D., Hannon, G., Barnekow, L., Wohlfarth, B., 2005. Deglacial
757 vegetation succession and Holocene tree-limit dynamics in the Scandes Mountains,
758 west-central Sweden: stratigraphic data compared to megafossil evidence. *Review of*
759 *Palaeobotany and Palynology* 134, 129-151, doi:10.1016/j.revpalbo.2004.12.005.
760 Barnett, C., Dumayne-Peaty, L., Matthews, J.A., 2001. Holocene climatic change and tree-
761 line response in Leirdalen, central Jotunheimen, south central Norway. *Review of*
762 *Palaeobotany and Palynology* 117, 119-137.
763 Berger, A.L., 1978. Long term variations of daily insolation and Quaternary climate change.
764 *Journal of Atmospheric Science* 35, 2362-2367.
765 Berner, K.S., Koç, N., Divine, D., Godtliebsen, F., 2008. Decadal-scale Holocene sea surface
766 temperature record from the sub-polar North Atlantic: evaluating the effects of Bonds
767 icerafting episodes on the regional SSTs. *Paleoceanography* 23, PA2210,
768 doi:10.1029/2006PA001339.

769 Berner, K.S., Koç, N., Godtliebsen, F., 2010, High frequency climate variability of the
770 Norwegian Atlantic Current during the early Holocene period and a possible
771 connection to the Gleissberg cycle. *The Holocene* 20(2), 245–255,
772 doi:10.1177/0959683609350391.
773 Birks, H.J.B., Line, J.M.L., 1992. The use of rarefaction analysis for estimating palynological
774 richness from Quaternary pollen-analytical data. *The Holocene* 2, 1-10.
775 Björck, S., Rundgren, M., Ingólfsson, Ó., Funder, S., 1997. The Preboreal oscillation around
776 the Nordic Seas: terrestrial and lacustrine responses. *Journal of Quaternary Science*
777 12, 455-465.
778 Bjune, A.E., 2005. Holocene vegetation history and tree-line changes on a north-south
779 transect crossing major climate gradients in southern Norway – evidence from pollen
780 and plant macrofossils in lake sediments. *Review of Palaeobotany and Palynology*
781 133, 49–275, doi:10.1016/j.revpalbo.2004.10.005.
782 Blaauw, M., 2010. Methods and code for 'classical' age-modelling of radiocarbon
783 sequences. *Quaternary Geochronology 5*, 512-518, doi:10.1016/j.quageo.2010.01.002.
784
785 Bond, G., Showers, W., Cheseby, M., Lotti, R., Almasi, P., de Menocal, P., Priore, P., Cullen,
786 H., Hajdas, I., Bonani, G., 1997. A pervasive millennial-scale cycle in the North
787 Atlantic Holocene and glacial climates. *Science* 294, 2130-2136.
788 Bond, G., Kromer, B., Beer, J., Muscheler, R., Evans, M.N., Showers, W., Hoffmann, S.,
789 Lotti-Bond, R., Hajdas, I., Bonani, G., 2001. Persistent solar influence on North
790 Atlantic climate during the Holocene. *Science* 278, 1257-1266,
791 doi:10.1126/science.1065680.
792 Bos, J.A.A., van Geel, B, van der Plicht, J, Bohncke, S., 2007. Preboreal climate oscillations
793 in Europe: Wiggle-match dating and synthesis of Dutch high-resolution multi-proxy
794 records. *Quaternary Science Reviews* 26, 1927–1950,
795 doi:10.1016/j.quascirev.2006.09.012.

796 Brynjolfsson, S., Schomacker, A., Ingolfsson, O., Keiding, J.K., 2105. Cosmogenic ^{36}Cl
797 exposure ages reveal a 9.3 ka BP glacier advance and the Late Weichselian-Early
798 Holocene glacial history of the Drangajökull region, northwest Iceland. *Quaternary*
799 *Science Reviews* 126, 140-157, doi:10.1016/j.quascirev.2015.09.001.
800 Budja, M., 2007. The 8200 cal yrs. BP "climate event" and the process of neolithisation in
801 south-east Europe. *Documenta Praehistorica* XXXIV, 191-201.
802 Burjachs, F., Jones, S.E., Giralt, S., Fernandez-Lopez de Pablo, J., 2016. Lateglacial to Early
803 Holocene recursive aridity events in the SE Mediterranean Iberian Peninsula: The
804 Salines playa lake case study. *Quaternary International* 403, 187-200,
805 doi:10.1016/j.quaint.2015.10.117.
806 Dahl, S.O., Nesje, A., Lie, Ø., Fjordheim, K., Matthews, J.A., 2002. Timing, equilibrium-line
807 altitudes and climatic implications of two early-Holocene glacier readvances during
808 the Erdalen Event at Jostedalsbreen, western Norway. *The Holocene* 12, 17–25,
809 doi:10.1191/0959683602hl516rp.
810 Daley, T.J., Thomas, E.R., Holmes, J.A., Street-Perrott, F.A., Chapman, M.R., Tindall, J.C.,
811 Valdes, P.J., Loader, N.J., Marshall, J.D., Wolff, E.W., Hopley, P.J., Atkinson, T.,
812 Barber, K.E., Fisher, E.H., Robertson, I., Hughes, P.D.M., Roberts, C.N., 2011. The
813 8200 yr BP cold event in stable isotope records from the north Atlantic region. *Global*
814 *and Planetary Change* 79, 288-302, doi:10.1016/j.gloplacha.2011.03.006.
815 Das, S.K., Routh, J., Roychoudhury, A.N., Val Klump, J., 2008. Elemental (C, N, H and P)
816 and stable isotope (δ^{15}N and δ^{13}C) signatures in sediments from Zeekoevlei, South
817 Africa: a record of human intervention in the lake. Journal of Paleolimnology 39, 349-
818 360, doi:10.1007/s10933-007-9110-5.
819 Davis, M.B., Moeller, R.E, Brubaker, L.B., 1984. Sediment focusing and pollen influx. In:
820 Haworth, E.Y, Lund, J.W.G. (eds.): *Lake sediments and environmental history*, 261-293.
821 University of Leicester, Leicester.

822 Davis, B.A.S., Stevenson, A.C., 2007.The 8.2 ka event and Early–Mid Holocene forests, fires
823 and flooding in the Central Ebro Desert, NE Spain. *Quaternary Science Reviews* 26,
824 1695-1712, doi:10.1016/j.quascirev.2007.04.007.
825 De Jonge, C., Hopmans, E.C., Stadnitskaia, A., Rijpstra, W.I.C., Hofland, R., Tegelaar, E.,
826 Sinninghe Damsté, J.S., 2013. Identification of novel penta- and hexamethylated
827 branched glycerol dialkyl glycerol tetraethers in peat using HPLC–MS^2, GC–MS and
828 GC–SMB-MS. *Organic Geochemistry* 54, 78-82,
829 doi:10.1016/j.orggeochem.2012.10.004.
830 De Jonge, C., Hopmans, E.C., Zell, C.I., Kim, J.-H., Schouten, S., Sinninghe Damsté, J.S.,
831 2014. Occurrence and abundance of 6-methyl branched glycerol dialkyl glycerol
832 tetraethers in soils: implications for palaeoclimate reconstruction. *Geochimica et*
833 *Cosmochimica Acta* 141, 97-112, doi: 10.1016/j.gca2014.06.013.
834 De Rosa, M., Gambacorta, A., 1988. The lipids of archaebacteria. *Progress in Lipid Research*
835 27, 153-175, doi: 10.1016/0163-7827(88)90011-2.
836 Deng, L., Jia, G., Jin, C., Li, S., 2016. Warm season bias of branched GDGT temperature
837 estimates causes underestimation of altitudinal lapse rate. *Organic Geochemistry* 96,
838 11-17, doi: 10.1016/j.orggeochem.2016.03.004.
839 DNMI, 2016. The Norwegian meteorological Institute,
840 http://sharki.oslo.dnmi.no/portal/page?_pageid=73,39035,73_39049&_dad=portal&_s
841 chema=PORTAL. Accessed April 2018.
842 Dormoy, I., Peyron, O., Combourieu Nebout, N., Goring, S., Kotthoff, U., Magny, M., Pross,
843 J., 2009. Terrestrial climate variability and seasonality changes in the Mediterranean
844 region between 15 000 and 4000 years BP deduced from marine pollen records.
845 *Climate of the Past* 5, 615-632, doi:10.5194/cp-5-615-2009.
846 Ertl, C., Pessi, A.-M., Huusko, A., Hicks, S., Kubin, E., Heino, S., 2012. Assessing the
847 proportion of "extra-local" pollen by means of modern aerobiological and
848 phenological records — An example from Scots pine (*Pinus sylvestris* L.) in northern

849 Finland. *Review of Palaeobotany and Palynology* 185, 1-12,
850 doi:10.1016/j.revpalbo.2012.07.014.
851 Fægri, K., Iversen, J., 1989. *Textbook of pollen analysis: 4th revised edition* by Fægri, K.
852 Kaland PE, Krzywinski K. Wiley,Chichester
853 Ficken, K.J., Li, B., Swain, D.L., Eglinton, G., 2000. An n-alkane proxy for the sedimentary
854 input of submerged/floating freshwater aquatic macrophytes. Org. Geochem. 31,
855 745–749, doi: 10.1016/S0146-6380(00)00081-4.
856 Fiłoc, M., Kupryjanowicz, M., Szeroczyńska, K., Suchora, M., Rzodkiewicz, M., 2017.
857 Environmental changes related to the 8.2-ka event and other climate fluctuations
858 during the middle Holocene: Evidence from two dystrophic lakes in NE Poland. *The*
859 *Holocene* 27(10), 1550-1566, doi: 10.1177/0959683617702233.
860 Gajewski, K., 1995. Modern and Holocene pollen assemblages from some small arctic lakes on
861 Somerset Island, NWT, Canada. *Quaternary Research* 44, 228-236.
862 Gavin, D.G., Henderson, A.C.G., Westover, K.S., Fritz, S.C., Walker, I.C., Leng, M.J., Hu,
863 F.S., 2011. Abrupt Holocene climate change and potential response to solar forcing in
864 western Canada. *Quaternary Science Reviews* 30, 1243-1255,
865 doi:10.1016/j.quascirev.2011.03.003.
866 Ghilardi, B., O'Connell, M., 2013. Early Holocene vegetation and climate dynamics with
867 particularreference to the 8.2 ka event: pollen and macrofossil evidence from a small
868 lake in western Ireland. *Vegetation History and Archaeobotany* 22, 99–114,
869 doi:10.1007/s00334-012-0367-x.
870 Gjerde, M., Bakke, J., Vasskog, K., Nesje, A., Hormes, A., 2016. Holocene glacier variability
871 and Neoglacial hydroclimate at Ålfotbreen, western Norway. *Quaternary Science*
872 *Reviews* 133, 28-47, doi: 10.1016/j.quascirev.2015.12.004.
873 Grime, J.P., 1973: Competitive exclusion in herbaceous vegetation. *Nature* 242, 344-347.
874 Grytnes, J.A., 2003. Species richness patterns of vascular plants along seven altitudinal
875 transects in Norway. *Ecography* 26, 291-300.

876 Gunnarsdottir, H., 1996. Holocene vegetation history and forest-limit fluctuations in
877 Smådalen, eastern Jotunheimen, South Norway. *Paläoklimaforshcung* 20, 233– 256.
878 Haflidason, H., Sejrup, H.P., Klitgaard Kristensen, D., Johnsen, S., 1995. Coupled response of
879 the late glacial climatic shifts of northwest Europe reflected in Greenland ice cores:
880 Evidence from the northern North Sea. *Geology* 23(12), 1059-1062.
881 Hicks, S., 2006. When no pollen does not mean no trees. *Vegetation History and*
882 *Archaeobotany* 15, 253–261, doi:10.1007/s00334-006-0063-9.
883 Hjelle, K.L., Halvorsen, L.S., Prøsch-Danielsen, L., Sugita, S., Paus, A., Kaland, P.E., Mehl,
884 I.K., Overland, A., Danielsen, R:, Høeg, H.I., Midtbø, I., 2018. Long-term changes in
885 regional vegetation cover along the west coast of southern Norway: The importance of
886 human impact. *Journal of Vegetation Science.* 12 pp*.,* doi: 10.1111/jvs.12626.
887 Holmes J.A., Tindall, J., Roberts, N., Marshall, W., Marshall, J.D., Bingham, A., Feeser, I.,
888 O'Connell, M., Atkinson, T., Jourdan, A.-L., March, A., Fisher, E.H., 2016. Lake
889 isotope records of the 8200-year cooling event in western Ireland: Comparison with
890 model simulations. *Quaternary Science Reviews* 131, 341-349, doi:
891 10.1016/j.quascirev.2015.06.027.
892 Hopmans, E.C., Weijers, J.W.H., Schefuß, E., Herfort, L., Sinninghe Damsté, J.S., Schouten,
893 S., 2004. A novel proxy for terrestrial organic matter in sediments based on branched
894 and isoprenoid tetraether lipids. *Earth and Planetary Science Letters* 224, 107-116,
895 doi: 10.1016/j.epsl.2004.05.012.
896 Hopmans, E.C., Schouten, S., Sinninghe Damsté, J.S., 2016. The effect of improved
897 chromatography on GDGT-based palaeoproxies. *Organic Geochemistry* 93, 1-6, doi:
898 10.1016/j.orggeochem.2015.12.006.
899 Jensen, C., Vorren, K.-D., Mørkved, B., 2007. Annual pollen accumulation rate (PAR) at the
900 boreal and alpine forest-line of north-western Norway, with special emphasis on
901 *Pinus sylvestris* and *Betula pubescens*. *Review of Palaeobotany and Palynology* 144,
902 337–361, doi:10.1016/j.revpalbo.2006.08.006.

903 Iriarte-Chiapusso, M.J., Munoz Sobrino, C., Gomez-Orellana, L., Hernandez-Beloqui, B.,
904 García-Moreiras, I., Fernandez Rodriguez, C., Heiri, O., Lotter, A.F., Ramil-Rego, P.,
905 2016. Reviewing the Lateglacial-Holocene transition in NW Iberia: A
906 palaeoecological approach based on the comparison between dissimilar regions.
907 *Quaternary International* 403, 211-236, doi: 10.1016/j.quaint.2015.09.029.
908 Kaland, P.E., Natvig, Ø. 1993. CORE 2.0., a computer program for stratigraphical data,
909 developed at University of Bergen, Norway. Unpublished
910 Kullman, L., 1986. Late Holocene reproductional patterns of *Pinus sylvestris* and *Picea*
911 *abies* at the forest limit in central Sweden. *Canadian Journal of Botany* 64, 1682–
912 1690, doi:10.1139/b86-225.
913 Kullman, L., 2005. Pine (*Pinus sylvestris*) treeline study dynamics during the past millennium
914 – a population study in west-central Sweden. *Annales Botanici Fennici* 42, 95-106.
915 Kullman, L., 2013. Ecological tree line history and palaeoclimate - review of megafossil
916 evidence from the Swedish Scandes. *Boreas* 42, 555-567, doi:10.1111/bor.12003.
917 Loomis, S.E., Russell, J.M., Ladd, B., Street-Perrott, F.A., Sinninghe Damsté, J.S., 2012.
918 Calibration and application of the branched GDGT temperature proxy on East African
919 lake sediments. *Earth and Planetary Science Letters* 357–358, 277-288, doi:
920 10.1016/j.epsl.2012.09.031.
921 Moran, A.P., Kerschner, H., Ochs, S.I., 2016. Redating the moraines in the Kromer Valley
922 (Silvretta Mountains) – New evidence for an early Holocene glacier advance. *The*
923 *Holocene* 26(4), 655-664, doi: 10.1177/0959683615612571
924 Moore, P.D., Webb, J.A., Collinson, M.E., 1991. *Pollen analysis.* Blackwell Scientific
925 Publications, Oxford.
926 Naafs, B.D.A., Inglis, G.N., Zheng, Y., Amesbury, M.J., Biester, H., Bindler, R., Blewett, J.,
927 Burrows, M.A., del Castillo Torres, D., Chambers, F.M., Cohen, A.D., Evershed, R.P.,
928 Feakins, S.J., Gałka, M., Gallego-Sala, A., Gandois, L., Gray, D.M., Hatcher, P.G.,
929 Honorio Coronado, E.N., Hughes, P.D.M., Huguet, A., Könönen, M., Laggoun-

930 Défarge, F., Lähteenoja, O., Lamentowicz, M., Marchant, R., McClymont, E.,
931 Pontevedra-Pombal, X., Ponton, C., Pourmand, A., Rizzuti, A.M., Rochefort, L.,
932 Schellekens, J., De Vleeschouwer, F., Pancost, R.D., 2017. Introducing global peat-
933 specific temperature and pH calibrations based on br-GDGT bacterial lipids.
934 *Geochimica et Cosmochimica Acta* 208, 285-301, doi: 10.1016/j.gca2017.01.038
935 Nesje, A., 1992. A piston corer for lacustrine and marine sediments. *Arctic Alpine Research* 24,
936 257-259.
937 Nesje, A., Dahl, S.O., 2001. The Greenland 8200 cal. yr BP event detected in loss-on-ignition
938 profiles in Norwegian lacustrine sediment sequences. *Journal of Quaternary Science*
939 16, 155–166.
940 Nesje, A., Kvamme, M., Rye, N., Løvlie, R. 1991. Holocene glacial and climate history of the
941 Jostedalsbreen region, western Norway; evidence from lake sediments and terrestrial
942 deposits. *Quaternary Science Reviews* 10, 87–114.
943 Nesje, A., Matthews, J.A., Dahl, S.O., Berrisford, M.S., Andersson, C., 2001. Holocene
944 glacier fluctuations of Flatebreen and winter-precipitation changes in the
945 Jostedalsbreen region, western Norway, based on glaciolacustrine sediment records.
946 *The Holocene* 11, 267–280.
947 Nesje, A., Dahl, S.O., Bakke, J., 2004. Were abrupt Lateglacial and early-Holocene climatic
948 changes in northwest Europe linked to freshwater outbursts to the North Atlantic and
949 Arctic Oceans? *The Holocene* 14(2), 299–310. doi.10.1191/0959683604hl708fa
950 Nicolussi, K., Schlüchter, C., 2012. The 8.2 ka event—Calendar-dated glacier response in the
951 Alps. *Geology* 40(9), 819-822, doi:10.1130/G32406.1
952 Obrochta, S.P., Miyahara, H., Yokoyama, Y., Crowley, T.J., 2012. A re-examination of
953 evidence for the North Atlantic "1500-year cycle" at Site 609. *Quaternary Science*
954 *Reviews* 55, 23-33, doi: 10.1016/j.quascirev.2012.08.008
955 Odland, A., 1996. Differences in the vertical distribution pattern of *Betula pubescens* in

956 Norway and its ecological significance. *Paläoklimaforschung* 20, 43-59. Gustav
957 Fischer Verlag, Stuttgart.
958 Ojala, A.K., Heinsalu, A., Kauppila, T., Alenius, T., Saarnisto, M., 2008. Characterizing
959 changes in the sedimentary environment of a varved lake sediment record in southern
960 central Finland around 8000 cal yr BP. *Journal of Quaternary Science* 23, 765–775,
961 doi:10.1002/jqs.1157
962 Paus, A., 2010. Vegetation and environment of the Rødalen alpine area, Central Norway,
963 with emphasis on the early Holocene. *Vegetation History and Archaeobotany* 19, 29-
964 51, doi:10.1007/s00334-009-0228-4
965 Paus, A., 2013. Human impact, soil erosion, and vegetation response lags to climate change:
966 Challenges for the mid-Scandinavian pollen-based transfer-function temperature
967 reconstructions. *Vegetation History and Archaeobotany* 22(3), 269 – 284,
968 doi:10.1007/s00334-012-0360-4
969 Paus, A., Haugland, V., 2017. Early- to mid-Holocene forest-line and climate dynamics in
970 southern Scandes mountains inferred from contrasting megafossil and pollen data. *The*
971 *Holocene* 27(3) 361–383, doi:10.1177/0959683616660172
972 Paus, A., Velle, G., Larsen, L., Nesje, A., Lie, Ø., 2006. Late-glacial nunataks in central
973 Scandinavia: biostratigraphical evidence for ice thickness from Lake Flåfattjønna,
974 Tynset, Norway. *Quaternary Science Reviews* 25, 1228-1246.
975 Paus, A., Velle, G., Berge, J., 2011. Late-glacial and early Holocene vegetation and
976 environment in the Dovre mountains, central Norway, as signaled in two Late-glacial
977 nunatak lakes. *Quaternary Science Reviews* 30, 1780-1793,
978 doi:10.1016/j.quascirev.2005.10.008
979 Paus, A., Boessenkool, S., Brochmann, C., Epp, L.S., Fabel, D., Haflidason, H., Linge, H.,
980 2015. Lake Store Finnsjøen - a key for understanding Late-Glacial/early Holocene
981 vegetation and ice sheet dynamics in the central Scandes Mountains. *Quaternary*
982 *Science Reviews* 121, 36-51, doi:10.1016/j.quascirev.2015.05.004

983 Peterse, F., Kim, J.-H., Schouten, S., Kristensen, D.K., Koç, N., Sinninghe Damsté, J.S.,
984 2009. Constraints on the application of the MBT/CBT palaeothermometer at high
985 latitude environments (Svalbard, Norway). *Organic Geochemistry* 40, 692-699, doi:
986 10.1016/j.orggeochem.2009.03.004
987 Punt, W. et al., 1976-1996. *The Northwest European Pollen Flora* (NEPF) Vol I (1976), Vol II
988 (1980), Vol III (1981), Vol IV (1984) Vol V (1988), Vol VI (1991), Vol VII (1996),
989 Elsevier, Amsterdam.
990 Rasmussen, P., Hede, M.U., Noe-Nygaard, N., Clarke, A.L., Vinebrooke, R.D., 2008.
991 Environmental response to the cold climate event 8200 years ago as recorded at Højby
992 Sø, Denmark. *Geological Survey of Denmark and Greenland Bulletin* 15, 57-60.
993 Rasmussen, S.O., Bigler, M., Blockley, S.P., Blunier, T., Buchardt, S.L., Clausen, H.B.,
994 Cvijanovic, I., Dahl-Jensen, D., Johnsen, S.J., Fischer, H., Gkinis, V., Guillevic, M.,
995 Hoek, W.Z., Lowe, J.J, Pedro, J.B., Popp, T., Seierstad, I.K., Steffensen, J.P,
996 Svensson, A.M., Vallelonga, P., Vinther, B.O., Walker, M.J.C., Wheatley, J.J.,
997 Winstrup. M., 2014. A stratigraphic framework for abrupt climatic changes during the
998 Last Glacial period based on three synchronized Greenland ice-core records: refining
999 and extending the INTIMATE event stratigraphy. *Quaternary Science Reviews* 106,
1000 14-28, doi: 10.1016/j.quascirev.2014.09.007
1001 Reimer, P.J., Bard, E., Bayliss, A., Beck, J.W., Blackwell, P.G. et al., 2013. INTCAL13 and
1002 MARINE13 radiocarbon age calibration curves 0-50,000 years cal yrs. BP.
1003 *Radiocarbon* 55, 1869-1887.
1004 Renssen H, Goosse H, Fichefet T (2007) Simulation of Holocene cooling events in a coupled
1005 climate model. *Quaternary Science Reviews* 26, 2019–2029,
1006 doi:10.1016/j.quascirev.2007.07.011
1007 Rohling, E.J., Pälike, H., 2005. Centennial-scale climate cooling with a sudden cold event
1008 around 8,200 years ago. *Nature* 43, 975–979, doi:10.1038/nature03421.

1009 Russell, J.M., Hopmans, E.C., Loomis, S.E., Liang, J., Sinninghe Damsté, J.S., 2018.
1010 Distributions of 5- and 6-methyl branched glycerol dialkyl glycerol tetraethers (br-
1011 GDGTs) in East African lake sediment: Effects of temperature, pH, and new lacustrine
1012 paleotemperature calibrations. *Organic Geochemistry* 117, 56-69, doi:
1013 10.1016/j.orggeochem.2017.12.003.
1014 Schouten, S., Hopmans, E.C., Pancost, R.D., Sinninghe Damsté, J.S., 2000. Widespread
1015 occurrence of structurally diverse tetraether membrane lipids: Evidence for the
1016 ubiquitous presence of low-temperature relatives of hyperthermophiles. *Proceedings*
1017 *of the National Academy of Sciences* 97, 14421-14426, doi:
1018 10.1073/pnas.97.26.14421.
1019 Schouten, S., Hopmans, E.C., Sinninghe Damsté, J.S., 2013. The organic geochemistry of
1020 glycerol dialkyl glycerol tetraether lipids: A review. *Organic Geochemistry* 54, 19-61,
1021 doi: 10.1016/j.orggeochem.2012.09.006.
1022 Seddon, A.W.R., Macias-Fauria, Willis., K.J., 2015. Climate and abrupt vegetation change in
1023 Northern Europe since the last deglaciation. *The Holocene* 25(1), 25-36, doi:
1024 10.1177/0959683614556383.
1025 Segerström, U., von Stedingk, H., 2003. Early Holocene spruce, *Picea abies* (L.) Karst., in
1026 west central Sweden as revealed by pollen analysis. *The Holocene* 13, 897–906,
1027 doi:10.1191/0959683603hl672rp.
1028 Selsing, L., 1998. Subfossils of Scots pine (*Pinus sylvestris* L.) from the mountain area of
1029 South Norway as the basis for a long tree-ring chronology. *Norsk Geografisk*
1030 *Tidsskrift* 52, 89-103.
1031 Seppä, H., 1998. Postglacial trends in palynological richness in the northern Fennoscandian
1032 tree-line area and their ecological interpretation. *The Holocene* 8, 43-53.
1033 Seppä, H., Hicks, S., 2006. Integration of modern and past pollen accumulation rate (PAR)
1034 records across the arctic tree-line: a method for more precise vegetation

reconstructions. *Quaternary Science Reviews* 25, 1501–1516, doi:10.1016/j.quascirev.2005.12.002.

Seppä, H., Birks, H. J. B., Giesecke, T., Hammarlund, D., Alenius, T., Antonsson, K., Bjune, A.E., Heikkilä, M., MacDonald, G.M., Ojala, A.E.K., Telford, R.J., Veski, S., 2007. Spatial structure of the 8200 cal yr BP event in northern Europe. *Climate of the Past* 3, 225-236.

Simonsen, A., 1980. Vertical variations of Holocene pollen sedimentation at Ulvik, Hardanger, SW-Norway (in Norwegian). *AmS-Varia* 8, 86 pp.

Sinninghe Damsté, J.S., Hopmans, E.C., Pancost, R.D., Schouten, S., Geenevasen, J.A.J., 2000. Newly discovered non-isoprenoid glycerol dialkyl glycerol tetraether lipids in sediments. *Chemical Communications*, 1683-1684, doi:10.1039/B004517I.

Sinninghe Damsté, J.S., Schouten, S., Hopmans, E.C., van Duin, A.C.T., Geenevasen, J.A.J., 2002. Crenarchaeol: the characteristic core glycerol dibiphytanyl glycerol tetraether membrane lipid of cosmopolitan pelagic crenarchaeota. *Journal of Lipid Research* 43, 1641-1651, doi:10.1194/jlr.M200148-JLR200.

Smith AG (1965) Problems of inertia and thresholds related to post Glacial habitat changes. *Proceedings of the Royal Society London B* 161, 331-342.

Stockmarr, J., 1971. Tablets with spores in absolute pollen analysis. *Pollen Spores* 13, 615–621.

Stranne, C., Jakobsson, M., Björk, G., 2014. Arctic Ocean perennial sea ice breakdown during the Early Holocene Insolation Maximum. *Quaternary Science Reviews* 92, 123-132, doi:10.1016/j.quascirev.2013.10.022.

Stuiver, M., Reimer, P.J., Reimer, R.W., 2018. CALIB 7.1 [WWW program] at http://calib.org, accessed June 2018.

Terasmaë, J., 1951. On the pollen morphology of *Betula nana*. *Svensk Botanisk Tidskrift* 45, 358–361.

ter Braak, C.J.F., Smilauer, P., 1997- 2002. CANOCO for Windows, version 4.5 Biometrics – Plant Research International, Wageningen, the Netherlands.

Thoen, M.W., 2016. *Effekt og omfang av 9.7- og 8.2 kulde-eventene ved Store Finnsjøen på Dovrefjell.* Master thesis, University of Bergen, Norway. 47 pp. https://bora.uib.no/bitstream/handle/1956/15529/152904321.pdf?sequence=1&isAllowed=y

Troels-Smith, J., 1955. Karakterisering av løse jordarter. *Danmarks Geologiske Undersøgelse* IV. Række 3, 73 pp.

van der Horn, S.A., van Kolfschoten T., van der Plicht, J., 2015. The effects of the 8.2 ka event on the natural environment of Tell Sabi Abyad, Syria: Implications for ecosystem resilience studies. *Quaternary International* 378, 111-118, doi:10.1016/j.quaint.2015.04.005.

Velle, G., Larsen, J., Eide, W., Peglar, S., Birks, H.J.B., 2005. Holocene environmental history and climate of Råtåsjøen, a low-alpine lake in central Norway. *Journal of Paleolimnology* 33, 129-153.

Vinther, B. M., Buchardt, S.L., Clausen, H.B., Dahl-Jensen, D., Johnsen, S.J., Fisher, D.A., Koerner, R.M., Raynaud, D., Lipenkov, V., Andersen, K.K., Blunier, T., Rasmussen, S.O., Steffensen, J.P., Svensson, A.M., 2009. Holocene thinning of the Greenland ice sheet. *Nature* 461, 385-388, doi:10.1038/nature08355.

Wanner, H., Solomina, O., Grosjean, M., Jetel, M., 2011. Structure and origin of Holocene cold events. *Quaternary Science Reviews* 30, 3109-3123, doi:10.1016/j.quascirev.2011.07.010.

Weber, Y., De Jonge, C., Rijpstra, W.I.C., Hopmans, E.C., Stadnitskaia, A., Schubert, C.J., Lehmann, M.F., Sinninghe Damsté, J.S., Niemann, H., 2015. Identification and carbon isotope composition of a novel branched GDGT isomer in lake sediments: Evidence

for lacustrine branched GDGT production. *Geochimica et Cosmochimica Acta* 154, 118-129, doi:10.1016/j.gca2015.01.032.

Weijers, J.W.H., Schouten, S., van den Donker, J.C., Hopmans, E.C., Sinninghe Damsté, J.S., 2007. Environmental controls on bacterial tetraether membrane lipid distribution in soils. *Geochimica et Cosmochimica Acta* 71, 703-713, doi:10.1016/j.gca2006.10.003

Weijers, J.W.H., Bernhardt, B., Peterse, F., Werne, J.P., Dungait, J.A.J., Schouten, S., Sinninghe Damsté, J.S., 2011. Absence of seasonal patterns in MBT–CBT indices in mid-latitude soils. *Geochimica et Cosmochimica Acta* 75, 3179-3190, doi:10.1016/j.gca2011.03.015.

Weijers, J.W.H., Bernhardt, B., Peterse, F., Werne, J.P., Dungait, J.A.J., Schouten, S., Sinninghe Damsté, J.S., 2011. Absence of seasonal patterns in MBT–CBT indices in mid-latitude soils. *Geochimica et Cosmochimica Acta* 75, 3179-3190, doi:10.1016/j.gca2011.03.015..

Whittington, G., Edwards, K.J., Zanchetta, G., Keen, D.H., Bunting, M.J., Fallick, A.E., Bryant, C.L.,2015. Lateglacial and early Holocene climates of the Atlantic margins of Europe: Stable isotope, mollusc and pollen records from Orkney, Scotland. *Quaternary Science Reviews* 122, 112-130, doi:10.1016/j.quascirev.2015.05.026.

Wohlfarth, B., Schwark, L., Bennike, O.,Filimonova, L., Tarasov, P., Björkman, L., Brunnberg, L., Demidov, I., Possnert, G., 2004. Unstable early-Holocene climatic and environmental conditions in northwestern Russia derived from a multidisciplinary study of a lek-sediment sequence from Pichozero, southeastern Russian Karelia. *The Holocene* 14(5), 732-746, doi:10.1191/0959683604hl751rp.

Young, N.E., Briner, J.P., Rood, D.H., Finkel, R.C., Corbett, L.B., Bierman. P.R., 2013. Age of the Fjord Stade moraines in the Disko Bugt region, western Greenland, and the 9.3 and 8.2 ka cooling events. *Quaternary Science Reviews* 60, 76-90, doi:10.1016/j.quascirev.2012.09.028.

Yu, S.H., Colman, S.M., Lowell, T.W., Milne, G.A., Fisher, T.G., Breckenridge, A., Boyd, M., Teller, J.T., 2010. Freshwater Outburst from Lake Superior as a Trigger for the Cold Event 9300 Years Ago. *Science* 328, 1262-1266, doi:10.1126/science.1187860.

Zheng, Y., Zhou, W., Meyers, P.A., Xie, S., 2007. Lipid biomarkers in the Zoigê-Hongyuan peat deposit: indicators of Holocene climate changes in West China. Org. Geochem. 38, 1927–1940, doi: 10.1016/j.orggeochem.2007.06.012.

Zolitschka, B., Francus, P., Ojala, A.E.K., Schimmelmann, A. 2015. Varves in lake sediments - a review. *Quaternary Science Reviews* 117, 1-41.

Figure and table captions

Fig. 1: Maps of the Lake Finnsjøen and Lake Flåfattjønna areas. Numbers show altitudes in m a.s.l.

Fig. 2: Selected sediment features from the Finnsjøen core displayed along the linear age/depth model. From left: X-ray colour image, pollen-assemblage zones (PAZ), XRF scanning results of sediment density, K and Ca (cps: counts per second), loss-on-ignition (LOI), *Pinus* and *Pediastrum* percentages, C/N ratios, *n*-Alkanes (terrestrial organic matter and aquatic input), br-GDGT-based estimates of pH and mean annual temperatures (MATmr), mid-month summer solar insolation 60 ^{o}N (Berger, 1978), and temperature deviations from present in ^{o}C based on ^{18}O values from the Renland ice core, Greenland (Vinther et al., 2009), The 9.7, 9.3, and 8.2 cold events are shaded. The 8.2 event (*sensu lato*) is displayed by a tripartite development: the early precursor from ca. 8420 cal yrs. BP, the erosional phase from ca. 8225 cal yrs. BP, and the

recovery phase from ca. 8175 to ca. 8050 cal yrs. BP. Stippled red lines show the one cm thick sediment slice missing from the core (see section 3.1).

Fig. 3: a): Age-depth relationship for the Finnsjøen sediments. Grey area illustrates the 95% probability range. Two outliers marked with bold crosses, are recognized. The average linear sedimentation rate (white line) represents the preferred chronology (see section 3.3).
b): The floating varve chronology based on microscale patterns of the XRF sediment density graph and compared with the radiocarbon based age-depth chronology. The youngest part of the varve chronology is tentatively attached to the uppermost level 7600 cal yrs. BP dated by the radiocarbon-based age-depth model.

Fig. 4: Comparison of selected features from the Finnsjøen and Flåfattjønna merged data set. The 9.7 and 8.2 cold events are shaded. Radiocarbon-dated levels are marked in the Flåfattjønna age column. Shaded curves are 10x exaggerations of the scale.

Fig. 5: Pollen accumulation rates (PAR) for selected Finnsjøen taxa. Shaded curves are 10x exaggerations of the scale.

Fig. 6: Pollen percentage diagram from Finnsjøen. Calibrated dates are shown as mean probabilities (Stuiver et al., 2018). Shaded curves are 10x exaggerations of the scale.

Fig. 7: Detailed data of the 9.7 and 8.2 events at Finnsjøen. Figure displays scanning results (Xray colour image, sediment density, the elements K and Ca, loss-on-ignition (LOI), *Pinus,* and temperature deviation (^{o}C) from present based on ^{18}O values in Renland ice core, Greenland (Vinther et al., 2009). To the right, the enlarged sediment densities

during the 9.7 and 8.2 erosion layers show couplets of alternating maxima and minima values representing varves. Shading highlights the 9.7 and the 8.2 erosion layers.

Fig. 8: Plot of pollen taxa along the first two axes of the PCA of the merged pollen data set from Flåfattjønna and Finnsjøen. Merged data set includes 121 samples, 108 terrestrial taxa. Eigenvalues axis 1: 0.5020, axis 2: 0.1578, axis 3: 0.0896, axis 4: 0.0502. In the analysis, *Pinus* was treated as a passive taxon whereas loss-on-ignition (LOI) and palynological richness (PR) were included as environmental variables. See section 5.3 for ecological interpretations of the axes.

Fig. 9: PCA of spectra from Flåfattjønna (a) and Finnsjøen (b). Pollen assemblage zones (PAZ) follow Paus (2010) and Fig. 6. Levels in PAZ S-4 are not encircled. Figures show the general vegetation development and the 9.7 and 8.2 impacts on vegetation in a two-dimensional gradient space. See section 5.3 for ecological interpretations of the axes. The data from the two lakes are from the same time interval: 7600 - 10.700 cal yrs. BP.

Table 1: General features of the sites studied. Local temperatures are extrapolated from the nearest meteorological stations (DNMI, 2016) using a lapse rate of 0.6 ^{O}C change per 100 m.

Table 2: Description of the Finnsjøen sediment lithology.

Table 3: Results of seven AMS dates of plant macrofossils from Finnsjøen. Calibrated dates according to Stuiver et al. (2018) are shown with two standard deviations. When dating results appear as two or more intervals, the two extreme values define the interval displayed. Median probabilities are shown in brackets. Lab. reference

numbers of two outliers are marked with [A]: ETH-48538 [A] and TRa-4470 [A]. Dates previously published (Paus et al., 2015), are marked with an asterisk.

Table 4: Names, dates, and biostratigraphical features of the Finnsjøen local pollen assemblage zones (PAZ).

Fig.1

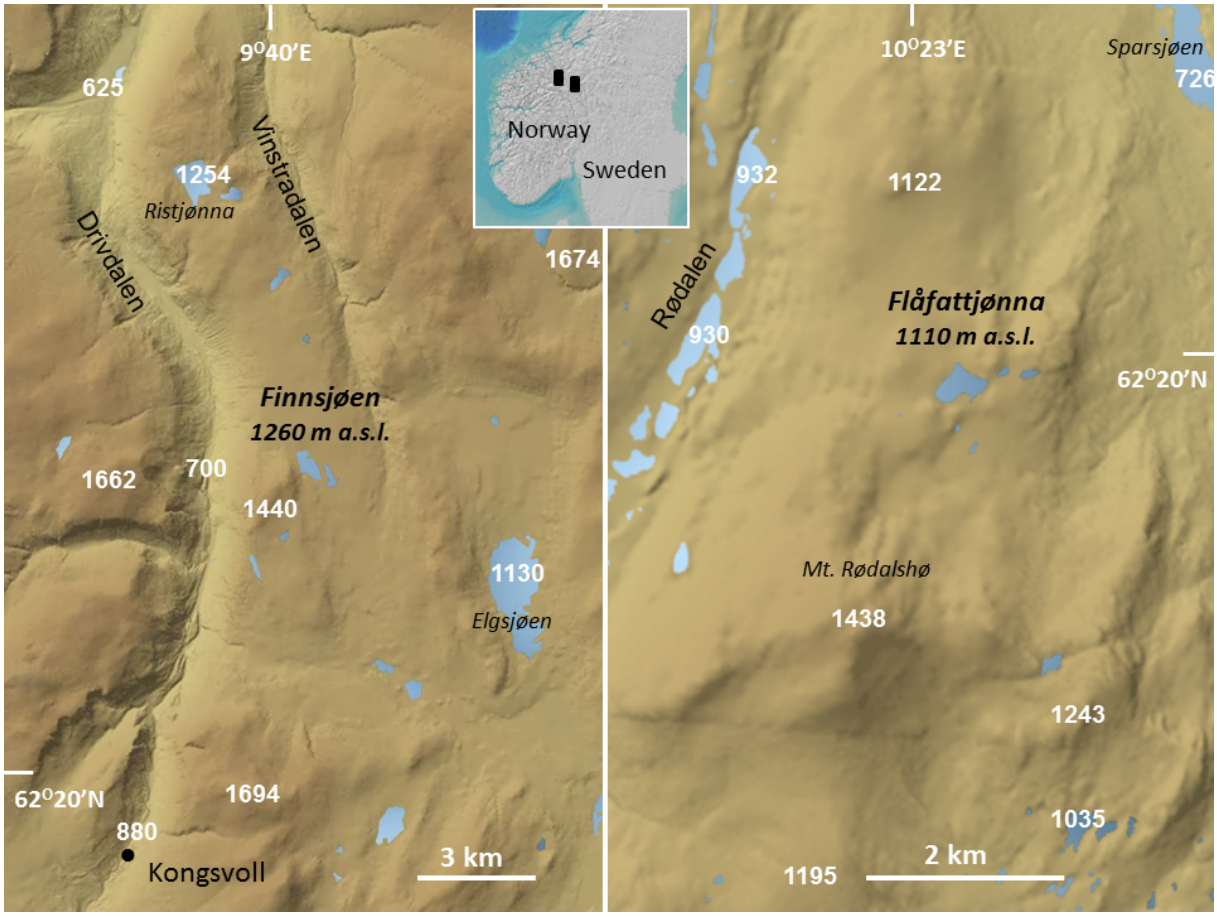

Fig.2

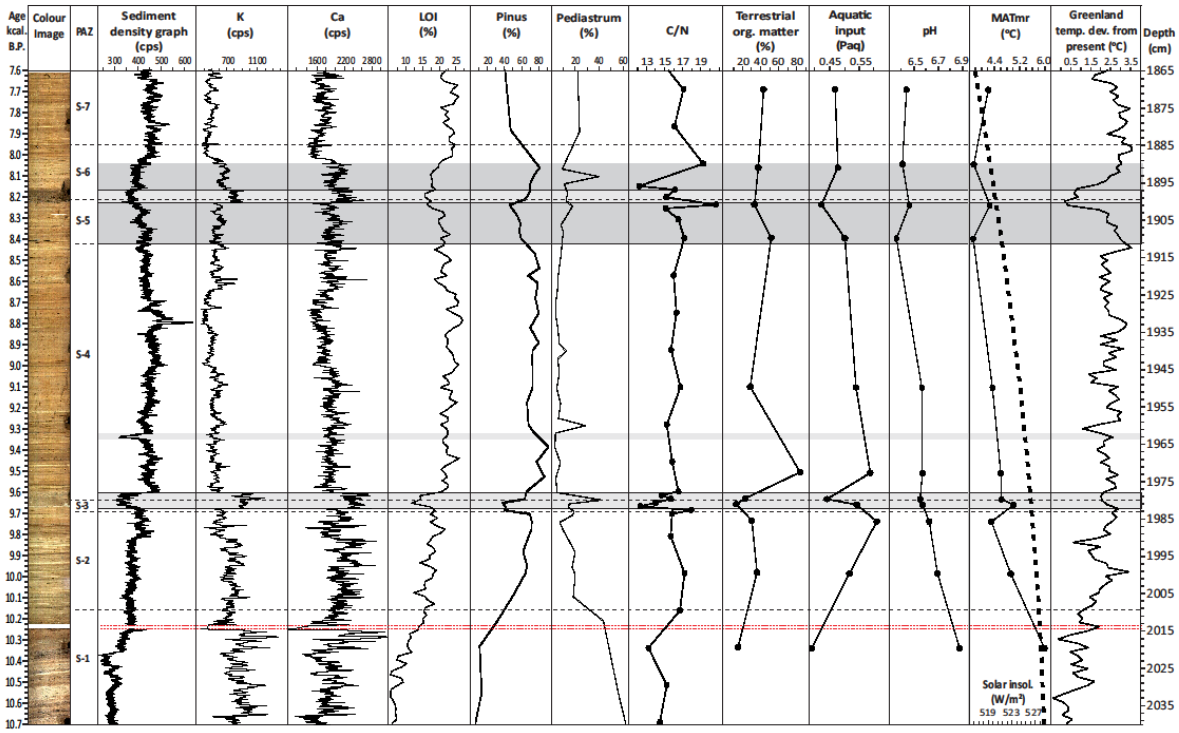

1201

1202 Fig 3.a

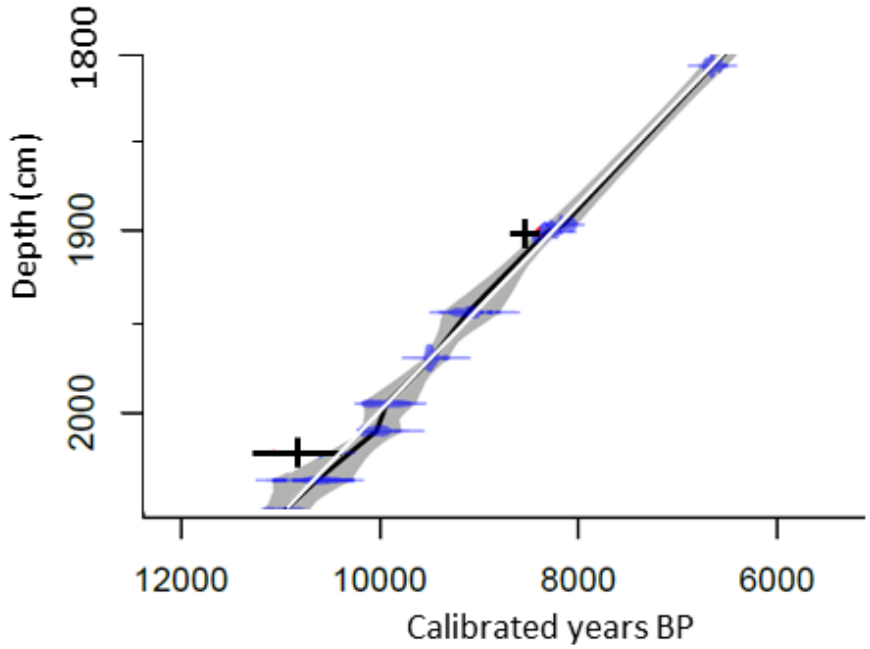

1203

1204

1205 Fig. 3b

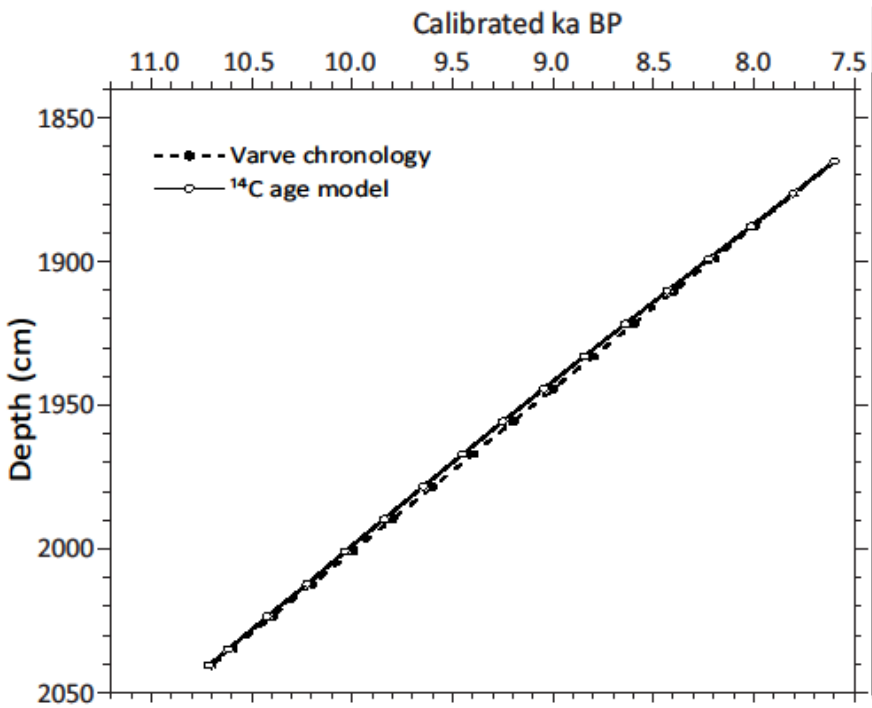

Depth (cm)	^{14}C Age model	Varve chronology
1865	7600	7600
1876	7800	7806
1888	8000	8015
1899	8200	8226
1910	8400	8433
1922	8600	8641
1933	8800	8847
1944	9000	9048
1956	9200	9250
1967	9400	9450
1978	9600	9648
1990	9800	9842
2001	10000	10038
2012	10200	10227
2024	10400	10424
2035	10600	10619
2040	10700	10717

1206

1207 Fig.4

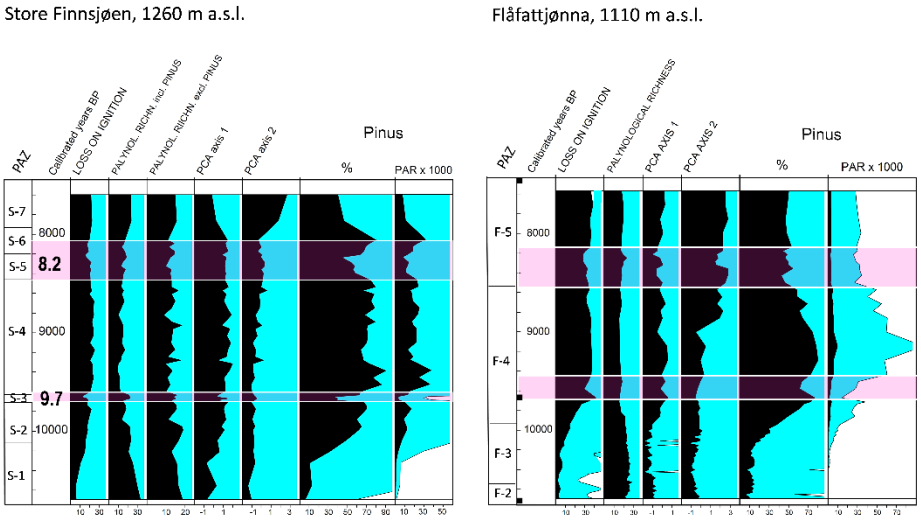

1208

1209 Fig. 5

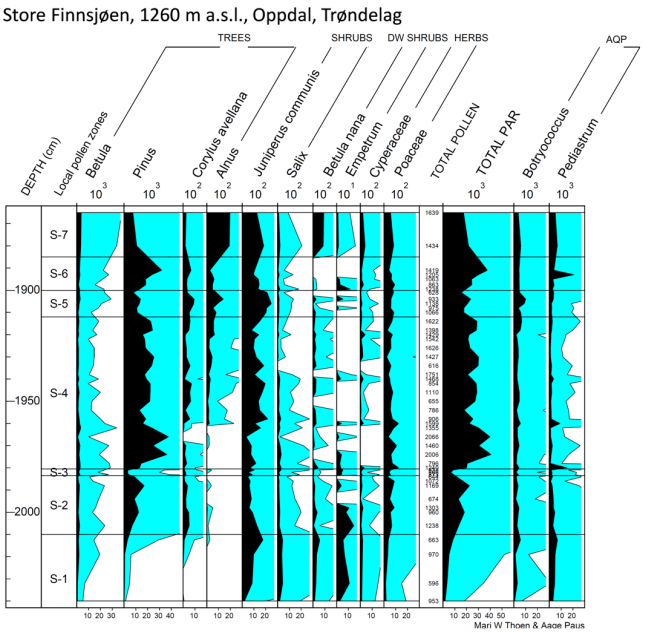

1210

1211 Fig. 6

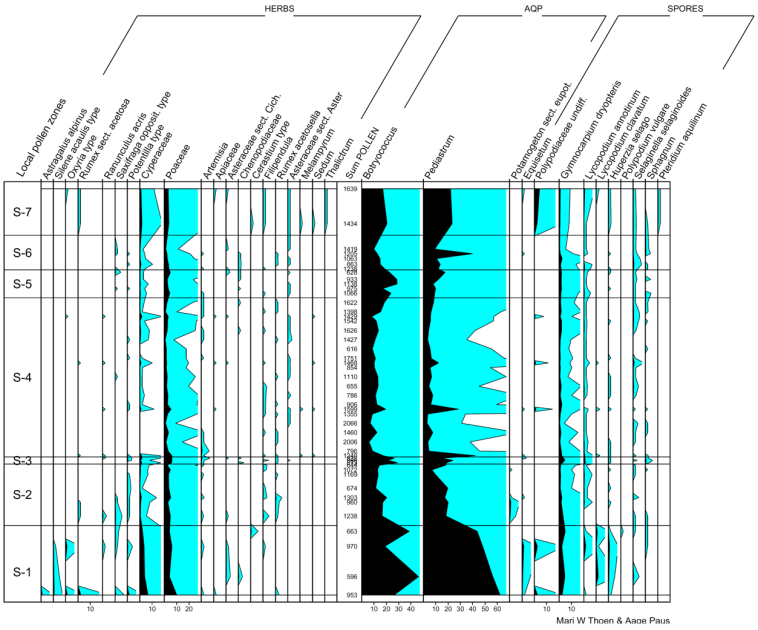

1212

1213

1214 Fig. 7

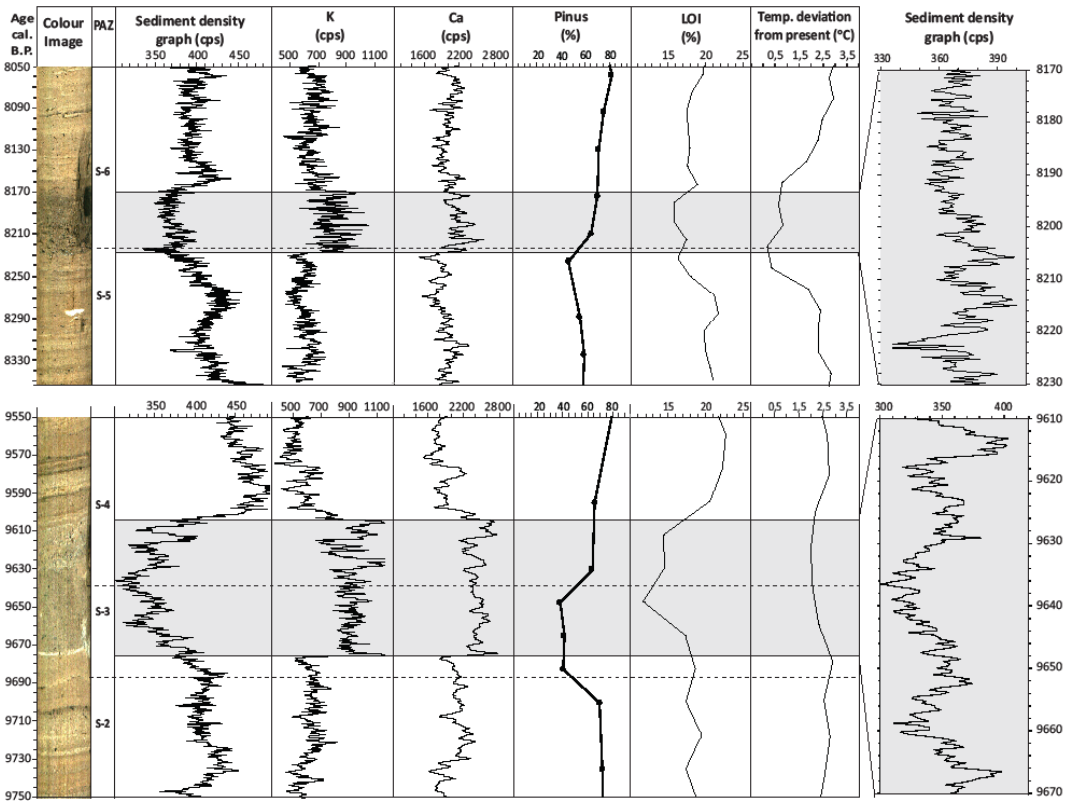

1215

1216

1217

1218 Fig.8

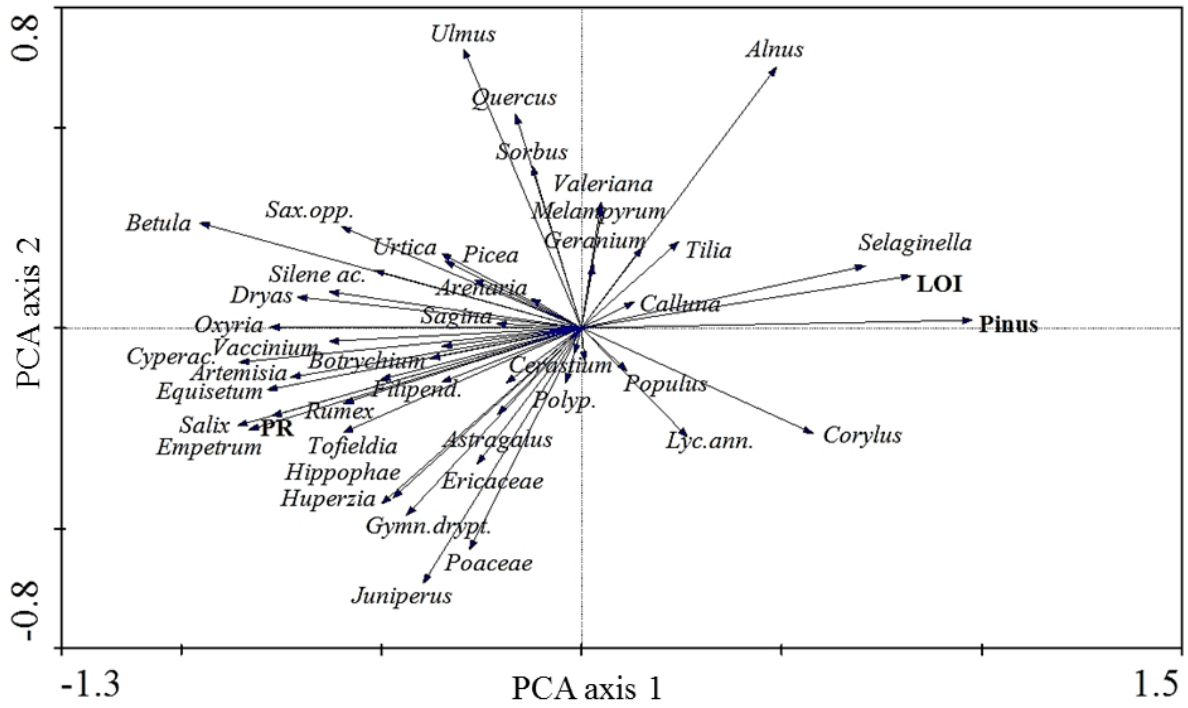

1219

1220 Fig. 9a

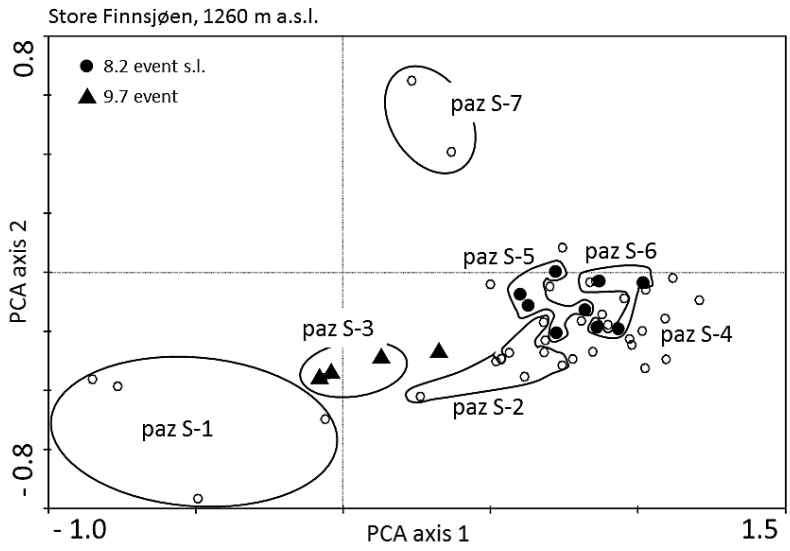

1221

1222

1223 Fig. 9b

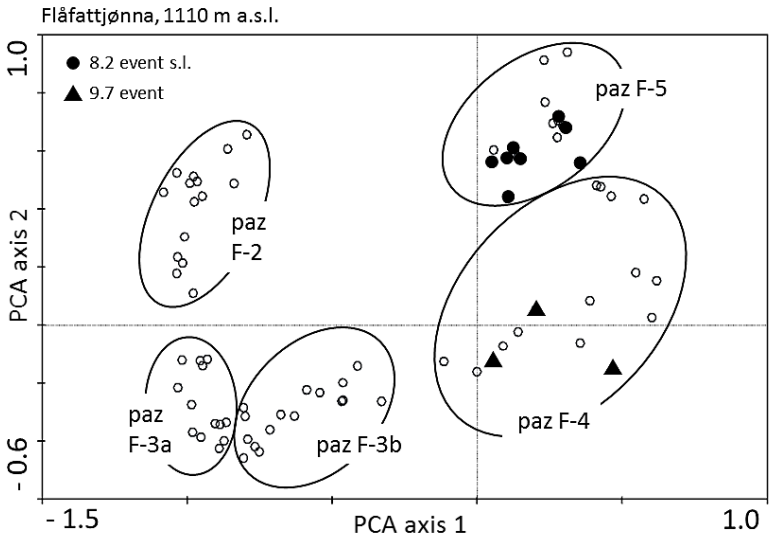

1224

1225

1226 Table 1

Table 1

	Lake Finnsjøen (1260 m a.s.l.)	Lake Flåfattjønna (1110 m a.s.l.)
Geographical position	62°24'N, 9°41'E	62°20'N, 10°24'E
Coring point position UTM 32V NQ	0535133 E 6918753 N	0572506 E 6911883 N
Basin size Basin area	800m x 390m 23.7 ha	425m x 225m 6 ha
Maximum water depth	14.7 m	13 m
Catchment size incl. basin	69 ha	25 ha
No of inlets /outlets	0 / 1	0 / 1
Local bedrock	greenschists, slate, amphibolite	Phyllite, micashists
July mean	7.5 ^{O}C	9 ^{O}C
January mean	-11.5 ^{O}C	-13 ^{O}C
Annual mean	-2.5 ^{O}C	-1.5 ^{O}C
Annual precipitation	450 mm	500 mm
Local birch-forest line	1100 m a.s.l.	1030 m a.s.l.
Local pine-forest line	900 m a.s.l.	820 m a.s.l.

1227

1228 Table 2.

Table 2

Depth (cm)	**Description (Troels-Smith 1955)**	**Colour**	**Comments**
1865-1898	Ld^3 3, Dh 1, Ag +	Dark brown (nig 3÷)	Laminated gyttja. Less laminated in the upper part. Distinct laminations rich in macrofossils are found at 1893 and 1867 cm. One distinct silty lamina occurs at 1885 cm.
1898-1901	Ld^4 2, Dh 1, Ag 1	Dark brown (nig 3+)	Silty layer rich in macrofossils and without laminations. Shining from mineral particles.
1901-1978	Ld^3 4, Dh +, Tb +, Ag +	Dark brown (nig 3)	Laminated gyttja, brown - grey brown in silty laminations. Distinct macro-layers at 1911, 1922, and 1963 cm. Distinct silt layers at 1921, 1929, 1957, 1960, and 1971 cm. One sand lens at 1904 cm
1978-1983	Ld^3 3, Ag 1	Grey brown (nig 3÷)	Unstratified silty gyttja
1983-2021	Ld^3 4, Dh +, Tb +, Ag +	Dark brown (nig 3)	Laminated gyttja with macro remains
2021-2040	Ld^2 2, Dh 1, Ag 1, As +	Brown (nig. 2+)	Laminated clay/silt gyttja. Includes several dark (nig 3) macrofossil-layers less than 1 cm thick. Most distinct between 2021 and 2023 cm ($Ld^2$1, Tb1, Dh1, Ag+). Two mm thick and light (nig 1) clay layer at 2026 cm depth.

1229

1230 Table 3.

1231

1232 Table 4.

1233

PAZ	Name	Age (cal. BP)	Pollen zone characteristics
S-7	*Alnus-Betula-Betula nana*	7580-7930	Pine declines to 45% ΣP and 10 10^3 grains cm^{-2} a^{-1}, respectively whereas *Alnus, Betula*, *Ulmus, Betula nana*, *Juniperus* and algae rise. Both palynological richness (PR) and LOI ri
S-6	*Pinus-Betula*	7930-8270	Pine percentages rise earlier than pine PAR, both reaching max values (82% ΣP, 41 10^3 gra cm^{-2} a^{-1}, respectively) in mid S-6. *Alnus, Betula*, *Juniperus* and PR show distinct minima. I early S-6, LOI drops to 15% and rises to 24% in late S-6.
S-5	*Alnus-Betula-Juniperus*	8270-8520	Pine declines and reaches a minimum (50% ΣP, 3 10^3 grains cm^{-2} a^{-1}) in late S-5. *Alnus, Betula, Corylus*, and juniper show maxima. PAR values for all taxa rapidly drops in late S- LOI and PR show no changes from S-4.
S-4	*Pinus-Betula-Populus*	8520-9680	Pine strongly rises to its Holocene maximum (90% ΣP, 45 10^3 grains cm^{-2} a^{-1}) at 9.4 ka BP thereafter pine slightly decrease. At 9.4 ka BP, *Alnus* establishes. In S-4, LOI reaches 20-2 whereas *Betula, Salix*, and algae drop to moderate values. PR reaches its Holocene minimu
S-3	*Betula-Juniperus-Salix*	9680-9730	Pine abruptly decreases to 40% and 3 10^3 grains cm^{-2} a^{-1}, total PAR reaches a minimum of 10^3 grains cm^{-2} a^{-1}, and LOI drops to 14%. *Betula, Juniperus, Salix*, and algae show distinc maxima, but their PAR values show no changes. PR reaches a maximum of 26.
S-2	*Pinus-Corylus*	9730-10,070	Early S-2 shows marked increases in pine (65-70%), LOI (20%), and total PAR (48 10^3 gra cm^{-2} a^{-1}). Tree-birch, juniper, *Empetrum, Betula nana*, and algae decrease. PAR and PR decrease in the last half of S-2.
S-1	*Betula-Juniperus-Salix*	10,070 – 10,670	Sparse pine (< 35 % ΣP) and distinct representation of *Betula*, shrubs/dwarf-shrubs, and al characterize S-1. Total PAR (< 6 10^3 grains cm^{-2} a^{-1}) and LOI (< 15%) are low. Palynologi richness (PR) is high (24-33) and includes many light-demanding pioneer taxa.

1234
1235